Published in final edited form as:

FASEB J. 2021 May ; 35(5): e21513. doi:10.1096/fj.202002799R.

Unique metabolic phenotype and its transition during maturation of juvenile male germ cells

Anna Laura Voigt[1], **Douglas Andrew Kondro**[1], **Diana Powell**[1], **Hanna Valli-Pulaski**[2], **Mark Ungrin**[1], **Jan-Bernd Stukenborg**[3], **Claudia Klein**[1], **Ian A. Lewis**[4], **Kyle E. Orwig**[2], **Ina Dobrinski**[1]

[1]Department of Comparative Biology and Experimental Medicine, Faculty of Veterinary Medicine, University of Calgary, Calgary, AB, Canada

[2]Department of Obstetrics, Gynecology and Reproductive Sciences, Magee-Womens Research Institute, University of Pittsburgh School of Medicine, Pittsburgh, PA, USA

[3]NORDFERTIL Research Lab Stockholm, Childhood Cancer Research Unit, Department of Women's and Children's Health, Karolinska Institutet and Karolinska University Hospital, Solna, Sweden

[4]Department of Biological Sciences, Faculty of Sciences, University of Calgary, Calgary, AB, Canada

Abstract

Human male reproductive development has a prolonged prepubertal period characterized by juvenile quiescence of germ cells with immature spermatogonial stem cell (SSC) precursors (gonocytes) present in the testis for an extended period of time. The metabolism of gonocytes is not defined. We demonstrate with mitochondrial ultrastructure studies via TEM and IHC and metabolic flux studies with UHPLC-MS that a distinct metabolic transition occurs during the maturation to SSCs. The mitochondrial ultrastructure of prepubertal human spermatogonia is shared with prepubertal pig spermatogonia. The metabolism of early prepubertal porcine spermatogonia (gonocytes) is characterized by the reliance on OXPHOS fuelled by oxidative decarboxylation of pyruvate. Interestingly, at the same time, a high amount of the consumed pyruvate is also reduced and excreted as lactate. With maturation, prepubertal spermatogonia show a metabolic shift with decreased OXHPOS and upregulation of the anaerobic metabolism-associated uncoupling protein 2 (UCP2). This shift is accompanied with stem cell specific

Correspondence Ina Dobrinski, Department of Comparative Biology and Experimental Medicine, Faculty of Veterinary Medicine, Department of Biochemistry and Molecular Biology, Cumming School of Medicine, University of Calgary, 404 HMRB, 3330 Hospital Dr. NW, Calgary, AB T2N 4N1, Canada., Idobrins@ucalgary.ca.

AUTHOR CONTRIBUTIONS

Conceptualization, A.L. Voigt and I. Dobrinski; Methodology, A.L. Voigt, D. Kondro, I. Dobrinski, D. Powell, Formal Analysis A.L. Voigt, D. Kondro, Investigation, A.L. Voigt, D. Kondro, D. Powell, H. Valli-Pulaski; Resources, I. Dobrinski, C. Klein, J. Stukenborg, K.E. Orwig, M. Ungrin, I.A. Lewis; Writing—Original Draft A.L. Voigt, Writing—Review and Editing, I. Dobrinski, K.E. Orwig, C. Klein, M. Ungrin, J. Stukenborg, H. Valli-Pulaski, I.A. Lewis; Visualization A.L. Voigt, D. Kondro; Supervision, I. Dobrinski; Funding Acquisition, I. Dobrinski.

CONFLICT OF INTERESTS

The authors declare no competing interests.

SUPPORTING INFORMATION

Additional Supporting Information may be found online in the Supporting Information section.

promyelocytic leukemia zinc finger protein (PLZF) protein expression and glial cell-derived neurotropic factor (GDNF) pathway activation. Our results demonstrate that gonocytes differently from mature spermatogonia exhibit unique metabolic demands that must be attained to enable their maintenance and growth in vitro.

Keywords

maturation; metabolism; prepubertal spermatogonia; reactive oxygen species

1 | INTRODUCTION

Spermatogonial stem cells (SSCs) are the basis of life-long spermatogenesis and male fertility. They reside within the seminiferous tubules of the testis in their niche at the basement membrane in very tight interaction with the surrounding somatic Sertoli cells. SSCs originate from primordial germ cells (PGCs). During embryonic formation of the mammalian testis, PGCs colonize the fetal gonad. At birth, PGCs have matured into gonocytes (prospermatogonia) in the testicular chords. During prepubertal development, gonocytes migrate from the center to the basement membrane of the testicular seminiferous tubules and mature to undifferentiated type A spermatogonia that include SSCs.[1–6] Functionally, the prepubertal maturation of SSCs is poorly characterized in humans due to the difficulties in obtaining tissue samples and the small number of germ cells that are present in immature testes. This highlights the need for model systems that appropriately reflect normal human development. Prepubertal maturation requires several years in humans and is characterized by immature SSC precursors.[7,8] In the mouse, prepubertal maturation occurs rapidly (<1 month)[2,7] and does not exhibit a juvenile pause, making it difficult to capture distinct maturation stages during SSC development. This difference in developmental timing limits the use of conventional rodent models for human reproduction research, underscoring the need for a robust in vitro model.

In the young prepubertal cancer patient, the germ cell pool of gonocytes and spermatogonia is highly sensitive to toxins and is often impaired by aggressive anti-cancer therapy.[9–16] As these patients do not produce sperm, semen samples cannot be cryopreserved. The isolation, expansion, and transplantation of spermatogonia could present an option to restore fertility.[9,10,17–22] Preservation of fertility will require large numbers of matured stem cells for efficient neospermatogenesis. Therefore, a thorough understanding of immature germ cell maturational processes is essential to facilitate the in vitro maintenance and propagation of functional stem cells.[23] Rodent germ cells used in in vitro studies are mainly harvested from prepubertal tissue, but rodent-specific culture conditions show limited success for higher mammalian and human germ cells.[18,24–26] Even under optimized conditions, the expansion of rodent germ cells in vitro is characterized by a small numbers of SSCs, high numbers of progenitor germ cells,[18,25,27] and a loss of stem cell potential over time.[28]

Recent studies of mouse SSCs indicated that glycolysis-optimized conditions improve stem cell expansion in vitro.[28] Glycolysis is activated via glia cell derived neurotrophic factor (GDNF) signaling pathways, an essential process for stem cell propagation in vivo and vitro.

[18,25,29–31] In some mouse strains (eg, C57BL/6), lower endogenous glycolysis activation is accompanied with lower in vitro proliferation of spermatogonia, and an increased activation of the GDNF and fibroblast growth factor (FGF) signaling pathways or glycolysis are required for their expansion in culture.[25,29]

In addition, transcriptional profiling of testicular cells suggests that SSCs rely on an anaerobic glycolysis-based metabolism[32–34] similar to other adult stem cells.[35–42]

However, stem cell metabolism can vary tremendously depending on developmental stage, cell location, and functional requirements as shown for pluripotent stem cells.[43–46]

We therefore hypothesized that the metabolic requirements for immature SSC precursors not yet settled within their niche microenvironment are different to those of mature stem cells. Our report establishes that early prepubertal spermatogonia have a prominent and unique mitochondrial phenotype and that porcine spermatogonia show high ultrastructural similarity to human spermatogonia. With limited access to immature human testis tissue for experimentation, we used the prepubertal pig, an animal model with a prepubertal phase lasting for several months[47] representative of the extended juvenile quiescence in human,[48] to investigate the metabolism of early prepubertal spermatogonia.

We demonstrate that early prepubertal spermatogonia rely on active mitochondrial respiration and undergo a metabolic shift towards a more anaerobic metabolism with testicular maturation. The shift was accompanied with PLZF protein translation and GDNF pathway activation. Our study establishes that a switch towards an anerobic metabolism and the change of mitochondrial dynamics accompany stem cell maturation. It underlines the importance for the investigation of immature tissue in an appropriate model with an extended reproductive developmental time course and is one step towards better defining the prepubertal phase in higher mammals and humans. Adapting in vitro systems to meet the specific metabolic requirements necessary for gonocyte maturation may ultimately enable downstream clinical applications for the preservation of fertility in survivors of childhood cancer.

2 | MATERIALS AND METHODS

2.1 | Animals and human subjects (samples)

Testes were obtained by castration of 1- and 8-week-old pigs (Sunterra Farms Ltd; Acme, AB, Canada, and the University of Alberta, Edmonton, AB). All procedures were performed with approval and under the oversight of the Animal Care Committee and the Institutional Review Board of the University of Calgary. Human samples were obtained from a previous study[49] (approved by the Committee for Ethics in Medical Research at the Karolinska Institutet, 2009/716-31/2) and from the Fertility Preservation Program in Pittsburgh with approval from the University of Pittsburgh Institutional Review Board (Protocol #STUDY09020220.) All experiments were performed with at least three biological replicates obtained from different individuals.

2.2 | Cell culture

Unless otherwise stated enriched or sorted cell populations were seeded in an optimized density of 90% surface coverage (150×10^3 cells/0.32 cm^2) and cultured in stem cell medium (Table S4) at 37°C, in 21% oxygen for metabolic analysis. Plates were treated with 100 µg/mL poly-D-lysine (Corning, NY, USA BioCoat Poly-D-Lysine, #354210) for 30 minutes. Enriched or sorted cells were immobilized to a monolayer with centrifugation at 45 G with no breaking and minimal acceleration. Medium height for oxygen consumption measurements was standardized as previously reported[50] (according to 500 µL per well for Agilent Seahorse XF 24 Cell Culture Plates [Agilent, Santa Clara, CA, USA]).

2.3 | Cell isolation

Germ cells were isolated by a two-step enzymatic digestion and enriched via differential plating as previously described[51] and subsequently purified by FACS for experiments comparing 1- and 8-week-old spermatogonia.

Comparisons between 1-week-old spermatogonia and Sertoli cells were performed with enriched cell populations (enriched by differential plating) with 81.29 ± 1.78% UCH-L1+ germ cells and 93.38 ± 1.17% GATA 4+ Sertoli cells (mean ± SEM). Flow cytometry life cell assays and all comparisons between early (1-week-old) and late (8-week-old) prepubertal spermatogonia were performed with cells enriched by FACS based on specific forward and side scatter properties (see Figure 2A, UCH-L1+ in red) as described[52] to a mean purity of 97.92 ± 0.77% (1-week-old) and 94.57 ± 1.4% UCH-L1+ (8-week-old).

2.4 | Mitochondrial membrane potential

Freshly purified cells were stained with 50 nM (200 nM for fixed cells) MitoTracker Deep Red (ThermoFischer, Waltham, MA,USA, #M22426) in a staining buffer (1:1 mix of DMEM/F12 and 1% BSA in PBS) or stained with 50 nM TMRE (ThermoFisher; #T669) in DMEM/F12 with 5% FBS, respectively, for 30 minutes at 37°C. Cells were treated with 10 µM CCCP (abcam, Cambridge, UK #ab141229) for 5 minutes before staining, and inhibitor was maintained in buffer throughout analysis as control. Cells of interest were subsequently analyzed via flow cytometry. MitoTracker Deep Red stained cells were fixed and additionally stained for UCH-L1 in 0.1% saponin and 0.1% BSA before analysis.

2.5 | Hydrogen peroxide stress test

Hydrogenperoxide stress test was performed with CellROX Flow Cytometry Kit (ThermoFisher C10492). Enriched cells were treated with increasing levels of H_2O_2 (0–400 µM). To measure oxidative stress, cells were incubated with 750 nM of CellROX for 30 minutes at 37°C and assessed using flow cytometry.

2.6 | Mitochondrial phenotype analysis

MitoTracker Deep Red (200 nM) and TOMM-20 (1:500) (Santa Cruz Biotechnology; #sc-17764) served to visualize mitochondria when imaged with a Leica TCS SP5 confocal microscope (Leica microsystems, Wetzlar, Germany). For transmission electron microscopy (TEM), samples were fixed in 2% paraformaldehyde and 2.5% glutaraldehyde in 0.1 M

cacodylate buffer at pH 7.4 for 2 hours at 4°C. After washing three times with the same buffer, the samples were postfixed in 1% osmium tetroxide buffered with cacodylate for 1 hours at room temperature, dehydrated through a graded series of acetone, and embedded in Epon resin. Ultrathin sections were cut in a Leica EM UC7 ultramicrotome using a diamond knife and stained with 2% aqueous uranyl acetate and Reynolds's lead citrate. The sections were observed in a Hitachi H7650 transmission electron microscope at 80 kV. The images were taken through an AMT600 digital camera mounted on the microscope. TEM pictures of mitochondria were analyzed for mitochondrial localization, orientation, and shape. Mitochondrial localization was categorized depending on mitochondria localization in relationship to each other into unilateral accumulated (majority of mitochondria are in under a mitochondria length distance to each other) or randomly distributed. Images with mitochondria categorized as unilaterally accumulated were further analyzed for orientation towards the basement membrane into two groups, depending on if the majority of the mitochondria bulk was in a <90° angle towards the basement membrane (Figure 1I). Mitochondria shape was analyzed with Image J for mean circularity. Statistical analysis was performed for mean circularity and % circularity </>0.7.

2.7 | Oxygen consumption rate and glycolytic flux

Oxygen consumption rate (OCR) and glycolytic flux (ECAR) assays were performed via XF24 Seahorse flux analyzer according to manufacturer's instructions (Agilent, North Billerica, MA, USA). Cells were seeded as a monolayer as described in 500 µL of medium. Respiration (OCR) was measured in OCR assay medium (Agilent; XF DMEM 102365-100) with oligomycin (2 µM; Enzo Life Sciences, Burlington, ON, Canada, #BML-CM111), mitochondrial uncoupling compound FCCP (4 µM; 2 µM for germ cell comparison; abcam, #ab141229), and respiratory chain inhibitor antimycin A (Abcam, #A8674) and rotenone (Enzo Life Sciences, #ALX-350-360) (1 µM each), and glycolytic function (extracellular acidification rate-ECAR) in ECAR medium (Agilent, XF DMEM Medium 103575-100) with 17.5-mM glucose, oligomycin (2 µM), and 2DG (100 mM, Sigma, #D8375)[29] (all Seahorse results are normalized to the number of cells per well (150×10^3 cells/0.32 cm^2; thereafter, all oxygen consumption rates harmonized accordingly and stated as pmol/min per 150×10^3 cells).

2.8 | Hypoxia assay

Hypoxia stress test was performed with a monolayer cell culture, and OCR was monitored with Oxygen Sensor Spots SP-PSt3-NAU (PreSens Regensburg, Germany). Medium height was standardized according to XF24 Seahorse flux analyzer experiments (500 to 750 µL in standard 24-well plates) as described.[50] Viability was assessed with PI and FDA.

2.9 | Metabolomic flux—UHPLC-MS

Extracellular flux studies were performed with an immobilized cell culture condition (150 000 cells in 300 µL of medium) as described above. Medium sampling timepoints from 12 to 48 hours were chosen for analysis. Metabolites were extracted from 50 µL medium in 950 µL 50% ice cold methanol to a dilution of D20 for 20 minutes on ice. Samples were centrifuged at 4°C at 21 000 G for 10 min. Supernatant was stored at -80°C. Intracellular flux studies were performed with non-immobilized (0.5×10^6) sorted 1- and 8-week-old

spermatogonia cultured in 500-µL DMEM (# D5030 Sigma, St. Louis, MO, USA) supplemented with ^{13}C glucose (10 mM), glutamine (4 mM), NaHCO3 (42.5 mM), HEPES (15 mM), dialyzed fetal bovine serum (10% v/v) over time.[35] Cells were resuspended in medium and either seeded or further processed within 15 minutes for timepoint (t0). Cells were harvested from plates and washed with PBS. Cell pellets were obtained by centrifugation at 500 G for 5 minutes at 4°C. Cell metabolites were extracted with 500 µL 90% methanol on ice for 20 minutes. Extract was centrifuged for 20 minutes at 21 000 G and 450 µL of supernatant was stored at -80°C. The day before analysis the extract was dried via vacuum centrifugation overnight and resuspended in 120 µL for analysis. Extracted metabolites from extracellular and intracellular studies were analyzed on a Q Exactive Hybrid Quadrupole-Orbitrap Mass Spectrometer coupled to a Vanquish Flex UHPLC System, integrated biocompatible system. Chromatographic separation was achieved on a Zorbax SB-C18 UHPLC column (2.1 mm × 50 mm × 1.8 um, Agilent, part number 822700-902) using a binary solvent system at a flow rate of 600 µL/min. Solvent A, 10-mM tributylamine, 10-mM acetate pH 7.5 in 97/3% (v/v) mass spectrometry grade water/methanol; Solvent B, mass spectrometry grade acetonitrile. The mass spectrometer was set in negative ion mode at a resolution of 140 000 scanning from 70 to 1000 *m/z*. The obtained data were analyzed using MAVEN software.[53,54] Compound identification was completed through the matching of previously characterized *m/z* and retention time properties of analytical standards.

2.10 | q-RT PCR

Gene expression of key glycolytic enzymes via q-PCR (Table S3) was assessed after FACS sorting of enriched spermatogonial populations as described.[52] RNA was extracted from 10^6 cells using RNeasy Mini Kit (Qiagen, Toronto, ON, Canada, #74104) and treated with DNase. For reverse transcription, 2 µg of total RNA was used for RT using MultiScribe Reverse Transcriptase (Applied Biosystems, ThermoFisher, #4311235). cDNA concentration was measured for each individual sample diluted 25-fold to a final amount of 2.55 ng for q-PCR using 7.500 Fast Real Time PCR System (Applied Biosystems, ThermoFisher Scientific, Burlington, ON, Canada), SsoFast Eva Green Supermix with Low ROX (Bio-Rad, Mississauga, ON, Canada #172-5211). Gene expression was analyzed after normalized to the mean of internal controls (HPRT1, RPL4, EIFl3).

2.11 | Western-blot

Cells were harvested and rinsed with PBS. Cell lysate was collected after incubation of cells with RIPA buffer containing protease inhibitor cocktail (Sigma, # P8340) on the ice for 30 minutes followed by centrifuging at 14 000 G for 20 minutes at 4°C. Protein concentration was measured using DC Protein Assay Kit II (Bio-Rad, #500-0112). The equal amount of total protein from each sample was then mixed with SDS loading buffer and boiled at 95°C for 5 minutes. The target proteins were separated by SDS-PAGE and then transferred onto PVDF membranes (Bio-Rad, #1620177). The membranes were blocked with 5% BSA/TBST with 0.1% Tween 20 and then incubated with primary antibodies listed in Table S2 at 4°C overnight. The membranes were washed with 1X TBST containing 0.1% Tween 20 and incubated with secondary antibodies for at least 1 h at room temperature. All secondary antibodies were diluted into 5% nonfat milk in 1X TBST with 0.1% Tween 20. The

membranes were washed with 1X TBST containing 0.1% Tween 20. ECL was carried out using Pierce ECL 2 Western Blotting Substrate (Thermo Fisher Scientific, #80196), and the signals were visualized with ChemiDoc XRS+ system (Bio-Rad, Mississauga, ON, Canada). The expression of HPRT1 was used as an internal control.

2.12 | Quantification and statistical analysis

The results are presented as mean ± SEM, if not otherwise stated, from at least three independent experiments (starting cell isolation from a pool of animals from 8-week-old vs. 1-week-old pigs, respectively). Biological replicates represent independently cultured cell population with three to 10 technical replicates. Normality was tested with Shaprio-Wilk test (if possible, by sample size via Anderson-Darling test, D'Agostino and Pearson test and Kolmogorov-Smirnov test); normality was assumed if all performed tests were indicating a normal distribution. Normally distributed data were analyzed with an unpaired parametric Student's *t* test; otherwise, a nonparametric *t* test (Mann-Whitney test) was used to compare ranks. Nested *t* tests were used for samples with a higher in-biological replicate than in between biological replicate variance. Unequal standard deviation was accounted for with Welch's correction. A value of $P < .05$ was considered statistically significant. GraphPad Prism 8.0 software was used for all statistical analyses.

3 | RESULTS

3.1 | Early prepubertal human and pig spermatogonia show high similarity in their distinct mitochondrial ultrastructure

The spermatogonial maturation in humans and higher mammals is functionally poorly defined. Gonocytes are hereafter referred to as early prepubertal spermatogonia. With our focus on the metabolism of early prepubertal human spermatogonia, we first employed transmission electron microcopy (TEM) and immunohistochemistry (IHC) of 3- to 9-month-old human testis to characterize the mitochondrial architecture in these cells. In the human testis under one year of age, early prepubertal spermatogonia were identified by their large nucleus and high nucleus to cytoplasm ratio. The cytoplasm of early prepubertal spermatogonia (gonocytes) was marked by prominent, round, and thick mitochondria accumulated in the perinuclear area (Figure 1A,C) and otherwise low electron density (ie, organelle density), which is in stark contrast to the electron dense cytoplasm of the surrounding Sertoli cells. These observations were confirmed by immunohistochemistry labeling for the outer mitochondrial membrane marker TOMM-20 (Figure 1B,D).

Our TEM studies revealed that mitochondria in early prepubertal spermatogonia were connected with intermitochondrial cement (nuage), a ribonucleoprotein dense structure accumulated between mitochondria[55,56]; Figure 1E). The mitochondria were predominantly round (91.61 ± 2.35 % of cells; with a cutoff of ≥0.7 circularity; of 462 mitochondria counted, $n = 7$ $p < .0001$; Figure S1A) with a mean circularity of 0.81 ± 0.005 (Figure S1B) in contrast to Sertoli cell mitochondria, which appeared longer and more compressed (Figure 1F).

To elucidate mitochondrial activity, we chose the prepubertal pig as an animal model with prolonged testicular maturation more representative of human developmental timing than rodent models.[47,57] The ultrastructure of prepubertal pig spermatogonia was similar to the situation in human testis (Figure 1G–K). Early prepubertal spermatogonia (from 1-week-old pig testes) were easily identified by TEM and IHC by their large nucleus and high nucleus to cytoplasm ratio (Figure 1G,H). In 1-week-old pig testis, the germ cells are mostly in the center of the seminiferous chord. As in human testis samples, the ultrastructure of early prepubertal pig spermatogonia was distinguished by round organelles surrounding the nucleus, which were identified as mitochondria via IHC-labeling for TOMM-20 (Figure 1H,J).

The majority of mitochondria in early prepubertal porcine spermatogonia was also round (85.36 ± 2.71% with circularity ≥ 0.70; of 1508 mitochondria counted, $n = 6$, $P < .0001$) with a mean circularity of 0.80 ± 0.005 (Figure S1B) and unilateral perinuclear accumulation (91.64 ± 3.25 %, $P = .0006$, $n = 7$) towards the basement membrane (77.73 ± 8.58 %, $P = .0035$, $n = 7$; Figures 1I and S1C). These mitochondria had a donut-like appearance containing an electron dense matrix (Figure 1K) in comparison to the branched, elongated, and tubule-shaped mitochondria of Sertoli cells (Figure 1L) with a mean circularity of 0.66 ± 0.02 ($n = 7$, $P < .0001$; Figure S1L).

Newborn (pnd 0) mouse gonocytes showed a similar ultrastructure phenotype (Figure S1F). However, because larger numbers of germ cells can be obtained for study from pig testes and reproductive maturation is more prolonged in pig and human development,[47,57–61] we proceeded to investigate the metabolism of early and late prepubertal pig spermatogonia to clarify the spermatogonial maturation events.

3.2 | Early prepubertal spermatogonia have high OXPHOS and low capacity for anaerobic glycolysis

Spermatogonia function in tight interaction with the somatic Sertoli cells. The metabolism of Sertoli cells is highly glycolytic, persistent during development and adulthood.[47,60–62] Therefore, we first focused on the metabolic assessment of early prepubertal (1-week-old) spermatogonia in comparison to Sertoli cells at the same age.

Mitochondrial membrane potential was assessed by flow cytometry for MitoTracker Deep Red. Our observations were surprising; early prepubertal spermatogonia (UCH-L1+) within the mixed population of cells isolated from seminiferous tubules of 1-week-old pig testes had high mitochondrial membrane potential (Figure 2A). The mitochondrial membrane potential assessed by tetramethyl rhodamine ethyl esther (TMRE) staining with flow cytometry was 1.74 ± 0.15-fold higher in spermatogonia than in age-matched Sertoli cells ($P = .02$, $n = 6$, Figure 2B). Accordingly, early prepubertal spermatogonia had significantly higher mitochondrial respiration, maximal respiration capacity, and respiration used for ATP production ($P < .006$, $n = 7$) than Sertoli cells assessed with the Seahorse Flux Analyzer (Figures 2C and S2C). Transcript analysis by qRT-PCR of 1-week-old pig testicular cells also revealed that early prepubertal spermatogonia displayed a significant upregulation in eight out of 10 differentially expressed (≥ 1.5-fold difference) OXPHOS-related genes in comparison to age-matched Sertoli cells (Figure 2D, $p < 0.027$, Table S1). Taken together,

these results indicate that early prepubertal spermatogonia contain highly active mitochondria and upregulated OXPHOS in comparison to Sertoli cells.

To address the possibility that these germ cells have an overall higher rate of metabolism than Sertoli cells, we next investigated the glycolytic activity of early prepubertal spermatogonia. Real-time assessment of the extracellular acidification rate (ECAR) with the Seahorse Flux Analyzer revealed that early prepubertal spermatogonia had significantly lower glycolysis and lower glycolytic capacity ($P < .0003$; $n = 3$; Figure 2E) than Sertoli cells. Indeed, the glycolytic reserve of Sertoli cells was 8.8-fold higher than in spermatogonia ($P < .0003$, $n = 3$; Figure S2D). That spermatogonia showed higher nonglycolytic acidification than Sertoli cells ($P = .0084$; $n = 3$) is a significant finding. The acidification is caused by mitochondrial CO_2 production during high respiration[63] and explains the high measured basal ECAR in spermatogonia compared to Sertoli cells. Respiration acidification is confirmed through a decrease of ECAR after blockage of ATP-synthase (complex V) with oligomycin (Figure 2E, red box) and its subsequent increase after inhibition of glycolysis with 2-deoxyglucose.

These results indicate that early prepubertal spermatogonia have a lower glycolytic flux than Sertoli cells and that the observed change in pH is mainly influenced by mitochondrial respiration rather than glycolytic flux.

To further elucidate this finding and test the anaerobic capacity of early prepubertal spermatogonia, the oxygen consumption rate of cells cultured in 24-well plates was continuously measured using optical oxygen sensor spots (PreSenS Oxygen Sensor). The OCR of these cultured cells was calculated using Fick's law as previously reported.[64] Within a 4-h culture period, early prepubertal spermatogonia again consumed significantly more oxygen than Sertoli cells ($P = .0011$; $n = 6$; Figure 2F). Exposure of Sertoli cells and spermatogonia to hypoxia (<0.2 % O_2 adjacent to the culture surface) for 24 hours did not cause a significant change in Sertoli cell oxygen consumption (Figure 2F) or viability (assessed with PI and FDA in ambient oxygen [21%] compared to hypoxic conditions and compared to initial viability; Figure S2E). In contrast, oxygen consumption in spermatogonia decreased to 79.25 ± 4.91 pmol/min/cells after 24 h of hypoxia ($P = .0001$, $n = 6$, Figure 2F), even lower than the consumption of Sertoli cells ($P = .0411$, $n = 6$; Figure 2F). This decline in respiration was accompanied by a 15.6 ± 1.79% decrease in cell viability compared to normoxic conditions ($P = .0175$, $n = 4$) and a decrease of 19.7 ± 2.65 % ($P = .0064$, $n = 4$) compared to initial viability. Under normoxic conditions, no significant decreases in OCR and viability in comparison to initial conditions were detected in spermatogonia (Figure S2F,G).

Taken together, our results show that, unlike Sertoli cells, early prepubertal spermatogonia cannot successfully maintain their viability under hypoxic conditions and therefore have a limited capacity for anaerobic metabolism.

3.3 | Early prepubertal spermatogonia preferentially consume pyruvate for subsequent oxidative decarboxylation and reduction

We next asked which metabolites are preferentially consumed during high mitochondrial metabolism in early prepubertal spermatogonia, performing extracellular flux studies, analyzed by UHPLC-MS. Figure 3A–C shows a representative time course of the metabolite consumption and production over a 48-h timespan.

Early prepubertal Sertoli cells were highly proliferative (20.9 ± 1.94 % overnight EdU incorporation after 48 hours of culture) and displayed considerably higher glucose consumption in comparison to pyruvate (glucose [3.53 ± 0.37 mM consumed in 48 hours; with 31.3 ± 7.2% of glucose remaining in medium after 48 hours, Figure S3A] vs. pyruvate [0.247 ± 0.05 mM consumed; 87.6 ± 2.5% of pyruvate left in medium, Figure S3B] P = .0001, n = 4; Figure 3A,C [representative time course of one biological replicate performed at multiple time points], Figure 3D quantification of all biological replicates [performed at 48 hours]).

Sertoli cells also produced high levels of lactate (4.33 ± 0.54 mM; Figure 3C,D).

Our data confirm that 1-week-old pig Sertoli cells have high glycolytic flux (>60% conversion of glucose to lactate), in agreement with existing literature.[62,65,66] This high glycolytic flux persists during development and adulthood, despite terminal differentiation of Sertoli cells and cessation of proliferation, which occurs at 3–4 months of age in pigs.[47,60–62]

Parallel cultures of low-proliferating early prepubertal spermatogonia (0.6 ± 0.09% overnight EdU incorporation after 48-h culture) consumed very low levels of glucose (0.147 ± 0.09 mM consumed; Figure 3A,D; with 97.1 ± 1.8 % glucose remaining in medium after 48 hours, Figure S3A). Yet substantial pyruvate consumption of 1.23 ± 0.16 mM was detected (Figure 3C,D; GC 38.5 ± 7.84% remaining in the medium, Figure S3B). This pyruvate intake was significantly higher than in Sertoli cells (P = .001, n = 4; Figure 3C).

We were intrigued by the finding that early prepubertal spermatogonia preferentially consumed pyruvate over glucose (Figure 3D, n = 4, P = .001), yet still produced 0.681 ± 0.1 mM of lactate within 48 h of culture (Figure 3C,D). We concluded that over 65% of the excreted lactate must originate from the metabolic reduction of the consumed pyruvate.

Together with the high mitochondrial membrane potential and elevated oxygen consumption rates, our data show that the oxidative decarboxylation of pyruvate within the TCA for subsequent OXPHOS is the primary source of energy for prepubertal spermatogonia in contrast to the energy demands of Sertoli cells, which are supported through glycolysis (Figure 3E). High pyruvate concentrations in the seminiferous tubules have been reported to originate from Sertoli cell secretion in vivo.[65–69]

3.4 | Early prepubertal spermatogonia have a high resistance to oxidative stress

To assess whether high mitochondrial activity was associated with high levels of oxidative stress caused by high activity of the electron transport chain during culture, we measured the

production of ROS/cell with CellROX Green dye using flow cytometry. No significant difference was detected between the highly glycolytic Sertoli cells and early prepubertal spermatogonia (Figure S4), yet another surprising piece of data. When we assessed transcript levels of enzymes for the cellular antioxidative machinery (Table S1), six of eight differentially expressed genes analyzed with qRT-PCR were expressed higher in early prepubertal spermatogonia compared to Sertoli cells ($P < .029$, $n = 4$; Figure 3E; Table S1).

We next performed an oxidative stress test by treating each cell population with hydrogen peroxide and subsequent assessment of cellular ROS levels as an indicator of antioxidative capacity and resistance to oxidative stress. Levels of ROS were significantly lower in early prepubertal spermatogonia than in early prepubertal Sertoli cells after 30 minutes of treatment with increasing concentrations of hydrogen peroxide (100–400 μM; $P < .033$, $n = 4$; Figure 3F). This allowed our group to confirm that early prepubertal spermatogonia have a highly efficient cellular antioxidative machinery.

Our studies establish that early prepubertal pig spermatogonia rely on a highly active mitochondrial metabolism, accompanied with high oxidative resistance and low anaerobic metabolic capacity. As this observation is different from what was reported for mouse pup (pnd 6–8) and adult spermatogonia,[28,29] we next investigated a potential metabolic transition during testicular maturation.

3.5 | Late prepubertal spermatogonia show a change in mitochondrial ultrastructure

At 8 weeks of age in the pig, spermatogonia are considered generally more mature. We therefore hereafter refer to 8-week-old pig-derived germ cells as late prepubertal spermatogonia. As in earlier stages, mitochondria in late prepubertal spermatogonia were located around the nucleus (Figure 4A–D, white arrow). Yet the cytoplasm of late prepubertal spermatogonia was characterized by higher electron density and the mitochondrial morphology was different from the early stage cells. Late prepubertal spermatogonia contained elongated mitochondria (47.9 ± 5.52% vs. 15.04 ± 2.75% elongated, cut off ≥ 0.7 circularity, $P = .0002$, $n = 5–7$, Figures 4E and S5A,B) with a significantly lower mean circularity of 0.66 ± 0.008 ($p < .0003$, $n = 5–7$; Figure S1B) compared to early prepubertal spermatogonia. Late prepubertal spermatogonia also contained well-structured endoplasmic reticulum that was closely associated with their mitochondria ($P = .002$, $n = 3–4$; Figure 4E). Specialized endoplasmic reticulum close to and connecting with mitochondria are known as mitochondria associated membranes (MAM).[56] MAM, a component of germ cell nuage, were more frequently observed than intermitochondrial cement in late prepubertal spermatogonia (Figure 4E, red arrowheads; Figure S5E, $P = .007$, $n = 3$). No obvious difference was seen in the mitochondria of Sertoli cells between both ages (Figure 4F).

3.6 | Late prepubertal spermatogonia have decreased mitochondrial activity

Spermatogonia from 8-week-old porcine tissue are more difficult to enrich than those from younger animals. For further metabolic flux analyses of early and late spermatogonia, germ cells from both ages were sorted by FACS after differential plating to achieve consistent purities between early and late prepubertal spermatogonia (purity ≥ 95%[52]).

Staining with MitoTracker Deep Red revealed that late prepubertal spermatogonia had >30% lower mitochondrial membrane potential than early prepubertal spermatogonia (mean intensity 44 664 ± 2479 vs. 31176 ± 919, $P = .012$, $n = 3$).

The lower mitochondrial membrane potential in late prepubertal spermatogonia was accompanied by lower basal respiration (159.8 ± 9.54 pmol/min/cells vs. 114.1 ± 9.93 pmol/min/cells, $P = .0293$, $n = 3$) and maximum respiration capacity (923.2 ± 104.5 vs. 459.9 ± 46.89 pmol/min/cells $P = .0155$, $n = 3$) compared to early prepubertal spermatogonia (Figures 4G and S6). Mitochondrial oxygen consumption for ATP production appeared higher in early prepubertal spermatogonia albeit not significantly different ($P = 0.056$, $n = 3$; Figure 4G).

Flow-sorted germ cells at both ages exhibited a slight decrease in mitochondrial respiration after sorting (Figures 2C and S2A). Nevertheless, mitochondrial activity clearly decreased with maturation of prepubertal spermatogonia.

3.7 | Late prepubertal spermatogonia show a metabolic transition towards glycolysis and differential gene expression similar to glycolytic Sertoli cells

Early and late prepubertal spermatogonia did not differ in proliferation over 48 hours of culture (0.6 ± 0.09 [1-week-old] vs. 0.86 ± 0.64 [8-week-old] % overnight Edu incorporation).

Although early prepubertal spermatogonia did not consume glucose, late prepubertal spermatogonia consumed 0.353 ± 0.17 mM glucose during the first 24 h of culture ($P = .043$; $n = 3$; Figure 5A,D). It was interesting to observe that this difference disappeared at 48 h of culture, when the glucose consumption of early prepubertal spermatogonia suddenly increased more than described above for nonsorted spermatogonia. At the same time, the pyruvate consumption and lactate production were slightly lower but remained otherwise consistent relative to each other in comparison to the non-sorted control (not sorted 48 h: glucose 0.147 ± 0.09 mM, pyruvate: 1.23 ± 0.16 mM, lactate: 0.681 ± 0.1 mM; sorted 48 hours: glucose: 0.668 ± 0.06 mM, pyruvate: 1.04 ± 0.15 mM, lactate: 0.500 ± 0.06 mM).

Although early prepubertal spermatogonia preferentially consumed pyruvate over the full 48 h of culture (Figure 5D,E 0.668 ± 0.06 mM glucose vs. 1.044 ± 0.16 mM of pyruvate consumption over 48 h, 24 h: $P = .0006$, 48 h: $P < .09$, $n = 3$), parallel cultures of late prepubertal spermatogonia did not show a difference in the pyruvate and glucose consumption over the same time span in vitro (0.669 ± 0.09-mM glucose vs. 0.613 ± 0.06-mM pyruvate consumption; Figure 5E). Therefore, during a 48-h culture period, early prepubertal spermatogonia consumed 0.430 ± 0.17 mM more pyruvate than late prepubertal spermatogonia ($P = .06$, $n = 3$; Figure 5B).

Our data highlight preferentially higher utilization of pyruvate in early prepubertal spermatogonia compared to late prepubertal spermatogonia, which showed a trend towards increased glucose metabolization relative to pyruvate.

Remarkably, at the same time, early prepubertal spermatogonia produced more lactate over 48 hours of culture ($P < .02$, $n = 3$, Figure 5D). However, as described above, this represents

mainly pyruvate reduction rather than glycolytic flux, as at 24 hours no glucose is consumed in early prepubertal spermatogonia, but more lactate is produced. Our data are supported by the higher pyruvate consumption of early prepubertal spermatogonia, which results in higher lactate production.

To further define differences in metabolic flux between the two age groups, we analyzed intracellular metabolic fluxes in cells incubated in U-C^{13}-glucose. In this experiment, the medium did not contain pyruvate to force cells to use glucose to allow assessment of the differential incorporation of glucose carbons in spermatogonia. We observed a high biological variance; however, throughout the time course of analysis, C^{13} incorporation was higher in late compared to early prepubertal spermatogonia (Figure 5F). Total percent C^{13} labeling of late prepubertal spermatogonia was 1.8 ± 0.29-fold at timepoint 12 hours (P = .12) and 1.63 ± 0.17-fold at time point 24 hours (P = .06) of the incorporation of earlier spermatogonial stages (n = 3; Figure 5F). Low cell numbers obtained after FACS cause high variability in C13 incorporation results; however, the results show a trend of a higher rate of glycolytic flux in late prepubertal spermatogonia compared to earlier stages accompanied with the loss of preferential pyruvate metabolization.

We next aimed to elucidate the underlying transcriptional profile and assessed metabolic enzymes of glycolysis, TCA, and oxidative phosphorylation by qRT-PCR (Table S1). Expression of lactate dehydrogenase *LDHC*, so far described for differentiating germ cells relying on OXPHOS,[70] was significantly upregulated in early prepubertal spermatogonia (2.13-fold higher at earlier stages; P = .002, n = 4; Table S1). Similar to what was observed in glycolytic Sertoli cells (4.6-fold higher *GAPDH* expression in Sertoli cells compared to early prepubertal spermatogonia), *GAPDH* gene expression (1.86-fold, P = .0004, n = 4; Figure 5G) and GAPDH protein (3.34-fold, P = .338, n = 4), assessed by western blot were significantly higher in late prepubertal spermatogonia than in early prepubertal spermatogonia (Figure 5G). Also, the expression of the anaerobic metabolism maintaining uncoupling protein 2 (*UCP2*) was 1.7-fold upregulated in late prepubertal spermatogonia (P = .003, n = 4; Figure 5G) in comparison to earlier stages by qRT-PCR. Similarly, glycolytic Sertoli cells showed 7.31-fold higher expression of *UCP2* compared to the early prepubertal spermatogonia. Isoforms of pyruvate dehydrogenase kinase (*PDK*) were not different between the two ages (Table S1).

These findings support the functional data suggesting the beginning of a metabolic transition towards an anaerobic metabolism in late prepubertal spermatogonia.

3.8 | Late prepubertal spermatogonia show increased sensitivity to ROS

Studies in the mouse showed the need for basic ROS levels and anaerobic metabolism for SSC replication.[28,29,71] Therefore, we were interested in the possibility of detecting a higher sensitivity to ROS in late prepubertal spermatogonia, similar to glycolytic Sertoli cells.

As in the case of glycolytic Sertoli cells, we also observed a lower expression in six out of 10 tested antioxidative enzymes in late compared to early prepubertal spermatogonia when assessed with qRT-PCR (P < .028, n = 4, Figure 5H; Table S1). Accordingly, late prepubertal spermatogonia showed lower resistance to hydrogen peroxide, with significantly higher ROS

levels ($P = .027$, $n = 3$) compared to early prepubertal spermatogonia after treatment with 400-μM H_2O_2 assessed via CellROX Green by flow cytometry (Figure 5I). These results indicate that the decrease in mitochondrial respiration is accompanied with a decreased antioxidative machinery and subsequent increased sensitivity towards ROS.

3.9 | The metabolic transition of late prepubertal spermatogonia is accompanied with upregulation of stem cell specific pathways

We next asked whether the observed change in metabolism is accompanied with an increased expression of SSC related genes and pathways. RT-qPCR assessment revealed that *PLZF* expression was 1.6-fold higher in late prepubertal spermatogonia than in early prepubertal spermatogonia ($P = .0169$, $n = 4$; Figure 6A). Interestingly, at the same time, expression of the transcription factor *C-Kit* was 3.95-fold higher in early prepubertal spermatogonia ($P = .0019$, $n = 4$, Figure 6A). Protein quantification with western blot detected PLZF protein in late prepubertal spermatogonia but not in early prepubertal spermatogonia ($P = 0.0027$, $n = 4$; Figure 6C). GFRA1 and RET protein levels were not different in western blot (Figure 6B).

The drastic difference in PLZF protein expression was accompanied by phosphorylation of AKT (Ser 473), which was not detected in early prepubertal spermatogonia ($P = .0416$, $n = 4$, Figure 6C). This result confirms the activity of the SSC self-renewal pathway through GDNF signalling in late prepubertal spermatogonia in contrast to earlier stages.

Germ cell maturation was also accompanied by an increase in histone H3 acetylation assessed by western blot (2.2-fold, $P = .0388$, $n = 4$, Figure 6B), generally associated with an open chromatin structure of stem cells. Acetyl-coenzyme A synthetase 2 (*ACSS2*), which increases acetylation in pluripotent stem cells,[72] was 2.7-fold higher expressed in late prepubertal spermatogonia compared to early prepubertal spermatogonia ($P = .032$, $n = 4$, Figure 6A), whereas expression of ATP citrate lyase *(ACLY)* was similar when analyzed with qRT-PCR (Table S1).

4 | DISCUSSION

Prepubertal reproductive development in humans spans a decade or more and is characterized by the existence of a juvenile gonadal quiescence.[73,74] The mechanisms that control spermatogonial maturation and metabolism in the prepubertal period are poorly described. Here, we characterize the unique metabolic phenotypes of developing prepubertal spermatogonia in a pig model chosen to resemble the prolonged prepubertal period in humans. Metabolism in early prepubertal spermatogonia in the 1-week old pig (structurally similar to those of an infant less than 1 year of age) are characterized by high mitochondrial respiration, preferential consumption of pyruvate over glucose, resistance to oxidative stress, and low anaerobic capacity. Spermatogonia from the 8-week-old pig (corresponding to late prepubertal spermatogonia in the human) display a metabolic shift towards anaerobic glycolysis with a decrease in pyruvate consumption and a relative increase in glucose metabolism that coincides with the upregulation of anaerobic metabolism-related enzymes and SSC maturation. These maturing prepubertal germ cells are also more sensitive to ROS.

Mature spermatogonia were long suspected to metabolize glucose.[68,75,76] Studies of mouse spermatogonia in culture showed a beneficial effect of glycolysis on SSC in vitro expansion and transplantation efficiency.[28,29] On the other hand, primordial germ cells (PGCs) that are the precursors of spermatogonia rely on high TCA flux and oxidative phosphorylation, and the TCA metabolite alpha-ketoglutarate (αKG) supports the in vitro induction of PGC-like cells from pluripotent stem cells.[77–79] In the developing gonad, PGCs differentiate into sex-specific gonocytes, which are present in the adluminal space of seminiferous tubules at the time of birth.[2,80] In this study, we referred to these cells as early prepubertal spermatogonia.

Based on gene expression analysis, the mechanisms underlying the change in metabolism in the germline during the initial postnatal phase might be distinct from what has been described in other stem cell types.[72,81,82] Although changes towards an anaerobic metabolism are often associated with an increase in pyruvate dehydrogenase kinase (PDK) activity, the expression of *PDK* isoforms was not different between the two spermatogonial ages. However, *GAPDH* expression was significantly higher in Sertoli cells and in more mature late prepubertal spermatogonia. GAPDH varies considerably during prenatal testicular development,[83] was previously considered a rate limiting enzyme of glycolysis in various germ cell stages,[84–87] and was enriched in mouse and human spermatogonial stem cell populations along with other glycolytic enzymes. [32,33,76] Therefore, GAPDH abundance and its regulation might play an important role in controlling the glucose metabolism in the germline and the testis. In addition, the uncoupling protein 2 (*UCP2*), a key metabolic enzyme for maintenance of an anaerobic metabolism,[88,89] was upregulated in Sertoli cells and also in late prepubertal spermatogonia.

Early prepubertal spermatogonia, which preferentially consume pyruvate over glucose, notably excrete high levels of lactate. The partial reduction of pyruvate to lactate is described in cells with high pyruvate catabolism and respiration independently of glucose availability, such as the early human embryo and meiotic spermatocytes[87,90] and may be necessary to maintain the intracellular redox homeostasis by production of NAD+.

In the mouse, the proliferation of SSCs is promoted by ROS production through NOX.[71,91] ROS are mainly produced by mitochondrial respiration.[92–95] Although the change towards OXPHOS with differentiation of ESCs was associated with an increase of antioxidative enzymes and ROS levels,[96] we observed that early prepubertal spermatogonia show high expression of antioxidative enzymes and a high resistance towards ROS, yet relatively low ROS levels. Lower ROS at a later time point of ESC differentiation[96] suggested that mitochondrial activity changes faster than the adjustments of the antioxidative machinery. Our results show that early prepubertal spermatogonia are well adjusted to their high mitochondrial activity.

The decreased expression of antioxidative enzymes and increased sensitivity to ROS in late prepubertal pig spermatogonia might be partially required for spermatogonial stem cell maturation. In mouse, spermatogonial maturation is already initiated prior to birth[97] and the first wave of spermatogenesis occurs 30 days postpartum. This may explain the different results emphasizing the importance of anaerobic glycolysis for maintenance in culture of SSCs obtained from mouse pups.[28,29] The metabolic transition from early prepubertal

spermatogonia/gonocytes relying on OXPHOS to more mature spermatogonia/SSCs with higher reliance on glycolysis occurs more slowly during the extended time span of testicular maturation in higher mammals compared to rodents. This difference necessitates awareness and potentially will require adjustments when working with immature spermatogonia from higher mammals and humans.

Several proteins are specifically expressed in mouse SSCs, including promyelocytic leukaemia zinc finger protein (PLZF), a member of the POK family of transcriptional repressors.[98] PLZF is essential for the maintenance of the spermatogonial stem cell pool[99,100] and already translated during gonocyte to spermatogonia maturation prior to birth in mice.[97] Glia cell derived neurotrophic factor (GDNF), required for spermatogonial stem cell self-renewal, facilitates its function through Src kinases and AKT.[101,102] Activation of the GDNF pathways is a hallmark of spermatogonial stem cell maturation rather than change of localization.[97] Neither the activation of the AKT pathway nor translation of PLZF was detected in early prepubertal spermatogonia in this study, yet both were present in late prepubertal spermatogonia. The data are indicative of developing stemness and parallels the ability of late but not early prepubertal porcine spermatogonia to reconstitute spermatogenesis after transplantation, a measure of SSC potential.[103]

Expression of *C-Kit* is important for primordial germ cell migration during embryonic development[104,105] and postnatal germ cell differentiation.[106–108] Accordingly, early prepubertal spermatogonia highly expressed *C-Kit* whereas expression was lower in later stages concomitantly with higher expression of PLZF that represses *C-Kit* expression.[109] PLZF can initiate a molecular “switch,”[98] which might be the precursor for the metabolic shift to anaerobic metabolism observed in our study. In this context, it is interesting to note that *Zfp145* (encoding PLZF) knock-out mouse models do not show reduced numbers of gonocytes, yet a progressive loss of the SSC pool.[99] PLZF counteracts the mammalian target of rapamycin (mTOR) via upregulation of Redd1,[110] which is important for mitochondrial activity and biogenesis[111] and responsible for low responsiveness to GDNF through a negative feedback in differentiating germ cells.[110] Moreover, mTOR negatively regulates autophagy. PLZF suppression of mTOR is crucial for high basal autophagy and the degradation of mitochondria for the maintenance of an anaerobic quiescent metabolism in hematopoietic stem cells.[112] Expression of PLZF might therefore mark the maturation of spermatogonia/SSCs and could be required for the maintenance of the anaerobic metabolism in SSCs.

The high mitochondrial activity of gonocytes is accompanied with round and thick mitochondria that accumulate around the nucleus. This distinct mitochondrial shape and localization are described in PGCs and fetal spermatogonia.[113–115] Our results showed that it was similar in 1-week-old pig and <1-year-old human germ cells, suggesting that the described metabolic phenotype is translatable to samples obtained from infant testes. Mitochondrial dynamics are essential for murine spermatogenesis.[55] Changes in mitochondrial shape and associated structures similarly accompanied the prepubertal stem cell maturation in pig testes. Mitochondria-associated structures, as part of the germ cell specific nuage, regulate various cellular functions in the germline. Nuage are ribonucleoprotein dense structures containing RNA binding proteins and regulating mRNA

translation and transposon silencing.[56,116] MAMs are particularly enriched with DAZL (deleted in azoospermia like), a germ cell-specific RNA binding protein,[56] known to facilitate effective translation of PLZF.[117,118] The ultrastructural changes of mitochondria-associated structures and beginning PLZF translation in late prepubertal spermatogonia observed in this study are potentially controlled by translational regulation of DAZL associated with MAMs.

Cell metabolism plays an important role in modulating the epigenetic profile, reprogramming or differentiation efficiency, and the cell fate.[72,89,112,119–121] The transition from PGCs to spermatogonia is accompanied with important epigenetic changes.[122–124] Epigenetic changes also occur at the same time as metabolic transitions during spermatogenesis.[125,126]

Histone (H3) acetylation is associated with an open chromatin structure and important for maintenance of other stem cells.[72,127] In the germline, H3-acetylation promotes stability of genes specifically expressed in undifferentiated spermatogonia[128] and increased acetylation was implicated in the metabolic shift towards anaerobic glycolysis in elongated spermatids.[125] Hence, the increase in H3-acetylation in late prepubertal spermatogonia observed in our study coincides with a transition in metabolism and the maturation to the stem cell. The transition of metabolism might therefore be one of the necessary driving forces for changes in the epigenetic landscape of the germline.

The unique metabolic phenotype of early prepubertal spermatogonia has implications for the handling and investigation of these cells. Common metabolic assays and techniques (such as measurement of glycolytic flux through extracellular lactate production or change of pH (ECAR) via the Seahorse Flux Analyzer) can be misleading in cells with high respiratory activity. Mitochondrial respiration was affected by cell sorting of early prepubertal spermatogonia, which might explain the sudden increase of glucose consumption after 24 hours as a compensatory mechanism of impaired mitochondrial respiration in these highly aerobically active early prepubertal spermatogonia. The effect of sorting on highly respiratory active cells and their mitochondrial metabolism requires further investigation.

In conclusion, early prepubertal spermatogonia rely on an aerobic metabolism that is accompanied with high resistance to ROS. Extracellular lactate levels originate largely from pyruvate reduction in these cells. With testicular maturation and migration of germ cells to the basement membrane there is a trend towards a more anaerobic metabolism with increased sensitivity towards ROS. To our knowledge, this is the first description of a distinct metabolic phenotype of early prepubertal spermatogonia and its change during maturation in a higher mammalian model with a prolonged prepubertal maturation phase more similar to humans and quite different from the situation in mice. Future research will serve to further elucidate the time course of this metabolic transition during prepubertal human development and the molecular mechanisms of metabolic and epigenetic changes, the maintenance of stemness in the germline, and alterations during culture. The connection between metabolism and function of immature stem cell progenitors described here might also be more broadly applicable to other stem cell systems. Understanding maturation of gonocytes to SSCs will help us to identify markers to reveal the timepoint of maturation in

infant individuals such that handling, and culture systems can be adapted to the maturation state of the male germ cells. This will be of translational importance to understand how supporting or manipulating the metabolism of immature germ cells in vitro can facilitate maintenance and gain of stem cell function in germ cells obtained from infants for preservation of future fertility.

Supplementary Material

Refer to Web version on PubMed Central for supplementary material.

ACKNOWLEDGMENTS

We thank Drs. Jeff Biernaskie and Timothy Shutt for critically reviewing the manuscript and Drs. Claude Kollin, Agneta Nordenskjöld, and Martin Ritzén for providing human testicular tissue samples. The work was supported by NIH/ORIP R01 OD016575 to I.D. and a Small Research Grant from the Alberta Children's Hospital Research Institute (A.L.V). Metabolomics data were acquired at the Calgary Metabolomics Research Facility (CMRF), which is supported by the International Microbiome Centre and the Canada Foundation for Innovation (CFI-JELF 34986). Human tissue acquisition was supported by R01 HD092084 to KEO. J.S. was supported by the Swedish Childhood Cancer Foundation (TJ2020-0026, PR2019-0123) and the Swedish Research Council (2018-03094). A.L.V. was supported by a German Fellowship Foundation Doctoral Scholarship. M.U. was supported by Alberta Children's Hospital Research Institute and Alberta Diabetes Institute.

Funding information

HHS | National Institutes of Health (NIH), Grant/Award Number: OD016575 and HD092084; Barncancerfonden (Swedish Childhood Cancer Foundation), Grant/Award Number: TJ2020-0026,PR2019-0123

Abbreviations:

ECAR	extracellular acidification rate
FGF	fibroblast growth factor
GC	germ cell
GDNF	glial cell-line derived neurotrophic factor
IHC	immunohistochemistry
MAM	mitochondria-associated membranes
OCR	oxygen consumption rate
OXPHOS	oxidative phosphorylation
PGC	primordial germ cells
PLZF	promyelocytic zinc finger protein
ROS	reactive oxygen species
SC	Sertoli cell
SSC	spermatogonial stem cell
TEM	transmission electron microscopy

TMRE	tetramethyl rhodamine ethyl esther
TOMM-20	translocase of outer mitochondrial membrane 20
UCP-2	uncoupling protein 2
UHPLC-MS	ultra-high-pressure liquid chromatography-mass spectrometry
UCH-L1	ubiquitin carboxy-terminal hydrolase L1

REFERENCES

1. Chiquoine AD. The identification, origin, and migration of the primordial germ cells in the mouse embryo. Anat Rec. 1954; 118(2):135–146. 10.1002/ar.1091180202. [PubMed: 13138919]
2. Culty M. Gonocytes, the forgotten cells of the germ cell lineage, birth defects research part C: embryo today. Reviews. 2009;87(1):1–26. 10.1002/bdrc.20142.
3. Manku G, Culty M. Mammalian gonocyte and spermatogonia differentiation: recent advances and remaining challenges. Reproduction. 2015;149(3):R139–R157. 10.1530/rep-14-0431. [PubMed: 25670871]
4. Molyneaux K, Wylie C. Primordial germ cell migration. Int J Develop Biol. 2004:48(5–6):537–543. 10.1387/ijdb.041833km.
5. Simkins CS. On the origin and migration of the so-called primordial germ cells in the mouse and the rat. Acta Zoologica. 1923;4(2–3):241–284. 10.1111/j.1463-6395.1923.tb00163.x.
6. Oatley JM, Brinster RL. Spermatogonial stem cells. Methods Enzymol. 2006;419(6):259–282. 10.1016/S0076-6879(06)19011-4. [PubMed: 17141059]
7. Wu X, Schmidt JA, Avarbock MR, et al. Prepubertal human spermatogonia and mouse gonocytes share conserved gene expression of germline stem cell regulatory molecules. Proc Natl Acad Sci USA. 2009;106(51):21672–21677. 10.1073/pnas.0912432106. [PubMed: 20018717]
8. Paniagua R, Nistal M. Morphological and histometric study of human spermatogonia from birth to the onset of puberty. J Anat. 1984;139(3):535–552. http://www.ncbi.nlm.nih.gov/pubmed/6490534%0Ahttp://www.pubmedcentral.nih.gov/articlerender.fcgi?artid=PMC1165067. [PubMed: 6490534]
9. Brinster RL, Zimmermann JW. Spermatogenesis following male germ-cell transplantation. Proc Natl Acad Sci USA. 1994;91 (24): 11298–11302. 10.1073/pnas.91.24.11298. [PubMed: 7972053]
10. Brinster RL, Avarbock MR. Germline transmission of donor haplotype following spermatogonial transplantation. Proc Natl Acad Sci. 1994;91 (24): 11303–11307. 10.1073/pnas.91.24.11303. [PubMed: 7972054]
11. Green DM, Zhu L, Wang M, et al. Effect of cranial irradiation on sperm concentration of adult survivors of childhood acute lymphoblastic leukemia: a report from the St. Jude Lifetime Cohort Study†, Hum Reprod. 2017;32(6):1192–1201. 10.1093/humrep/dex082. [PubMed: 28444255]
12. Levine J, Canada A, Stern CJ. Fertility preservation in adolescents and young adults with cancer. J Clin Oncol. 2010;28(32):4831–4841. 10.1200/jco.2009.22.8312. [PubMed: 20458029]
13. Wallace WHB, Anderson RA, Irvine DS. Fertility preservation for young patients with cancer: who is at risk and what can be offered? Lancet Oncol. 2005;6(4):209–218. 10.1016/s1470-2045(05)70092-9. [PubMed: 15811616]
14. Stukenborg J- B, Alves-Lopes JP, Kurek M, et al. Spermatogonial quantity in human prepubertal testicular tissue collected for fertility preservation prior to potentially sterilizing therapy. Hum Reprod. 2018;33(9): 1677–1683. 10.1093/humrep/dey240. [PubMed: 30052981]
15. Poganitsch-Korhonen M, Masliukaite I, Nurmio M, et al. Decreased spermatogonial quantity in prepubertal boys with leukaemia treated with alkylating agents. Leukemia. 2017;31(6):1460–1463. 10.1038/leu.2017.76. [PubMed: 28270690]
16. David S, Orwig KE. Spermatogonial stem cell culture in oncofertility. Urol Clin North America. 2020;47(2):227–244. 10.1016/j.ucl.2020.01.001.

17. Kubota H, Brinster RL. Technology Insight: in vitro culture of spermatogonial stem cells and their potential therapeutic uses. Nat Clin Pract Endocrinol Metabol. 2006;2(2):99–108. 10.1038/ncpendmet0098.

18. Kanatsu-Shinohara M, Ogonuki N, Inoue K, et al. Long-t erm proliferation in culture and germline transmission of mouse male germline stem cells, Biol Reprod. 2003;69(2):612–616. 10.1095/biolreprod.103.017012. [PubMed: 12700182]

19. Hermann BP, Sukhwani M, Winkler F, et al. Spermatogonial stem cell transplantation into rhesus testes regenerates spermatogenesis producing functional sperm. Cell Stem Cell. 2012;11(5):715–726. 10.1016/j.stem.2012.07.017. [PubMed: 23122294]

20. Ogawa T, Dobrinski I, Avarbock MR, Brinster RL. Transplantation of male germ line stem cells restores fertility in infertile mice. Nat Med. 2000;6(1):29–34. 10.1038/71496. [PubMed: 10613820]

21. Honaramooz A. Fertility and germline transmission of donor haplotype following germ cell transplantation in immunocompetent goats, Biol Reprod. 2003;69(4): 1260–1264. 10.1095/biolreprod.103.018788. [PubMed: 12801978]

22. Goossens E, Jahnukainen K, Mitchell RT, et al. Fertility preservation in boys: recent developments and new insights †. Hum Reprod Open. 2020;2020(3):hoaa016. 10.1093/hropen/hoaa016. [PubMed: 32529047]

23. Brinster RL, Nagano M. Spermatogonial stem cell transplantation, cryopreservation and culture. Semin Cell Develop Biol. 1998;9(4):401–409. 10.1006/scdb.1998.0205.

24. Ryu BY, Orwig KE, Kubota H, Avarbock MR, Brinster RL. Phenotypic and functional characteristics of spermatogonial stem cells in rats. Developmental Biology. 2004;274(1):158–170. 10.1016/j.ydbio.2004.07.004. [PubMed: 15355795]

25. Kubota H, Avarbock MR, Brinster RL. Growth factors essential for self-r enewal and expansion of mouse spermatogonial stem cells. Proc Natl Acad Sci USA. 2004;101(47):16489–16494. 10.1073/pnas.0407063101. [PubMed: 15520394]

26. Richardson TE, Chapman KM, Tenenhaus Dann C, Hammer RE, Hamra FK. Sterile testis complementation with spermatogonial lines restores fertility to DAZL-deficient rats and maximizes donor germline transmission, PLoS ONE. 2009;4(7):e6308. 10.1371/journal.pone.0006308. [PubMed: 19621088]

27. Kanatsu-Shinohara M, Inoue K, Ogonuki N, Morimoto H, Ogura A, Shinohara T. Serum- and feeder-free culture of mouse germline stem cells. Biol Reprod. 2011;84(1):97–105. 10.1095/biolreprod.110.086462. [PubMed: 20844279]

28. Helsel AR, Oatley MJ, Oatley JM. Glycolysis-optimized conditions enhance maintenance of regenerative integrity in mouse spermatogonial stem cells during long-term culture. Stem Cell Rep. 2017;8(5):1430–1441. 10.1016/j.stemcr.2017.03.004.

29. Kanatsu-Shinohara M, Tanaka T, Ogonuki N, et al. Myc/Mycn-mediated glycolysis enhances mouse spermatogonial stem cell self-renewal. Genes Develop. 2016;30(23):2637–2648. 10.1101/gad.287045.116. [PubMed: 28007786]

30. Kubota H, Avarbock MR, Brinster RL. Culture conditions and single growth factors affect fate determination of mouse spermatogonial stem cells. Biol Reprod. 2004;71(3):722–731. 10.1095/biolreprod.104.029207. [PubMed: 15115718]

31. Meng X, Lindahl ME, Hyvönen M, et al. Regulation of cell fate decision of undifferentiated spermatogonia by GDNF. Science. 2000;287(5457): 1489–1493. 10.1126/science.287.5457.1489. [PubMed: 10688798]

32. Guo J, Grow EJ, Mlcochova H, et al. The adult human testis transcriptional cell atlas. Cell Res. 2018;28(12):1141–1157. 10.1038/s41422-018-0099-2. [PubMed: 30315278]

33. Hermann BP, Cheng K, Singh A, et al. The mammalian spermatogenesis single-cell transcriptome, from spermatogonial stem cells to spermatids. Cell Rep. 2018;25(6):1650–1667.e8. 10.1016/j.celrep.2018.10.026. [PubMed: 30404016]

34. Sohni A, Tan K, Song HW, et al. The neonatal and adult human testis defined at the single-cell level. Cell Rep. 2019;26(6):1501–1517.e4. 10.1016/j.celrep.2019.01.045. [PubMed: 30726734]

35. Simsek T, Kocabas F, Zheng J, et al. The distinct metabolic profile of hematopoietic stem cells reflects their location in a hypoxic niche. Cell Stem Cell. 2010;7(3):380–390. 10.1016/j.stem.2010.07.011. [PubMed: 20804973]
36. Spangrude GJ, Johnson GR. Resting and activated subsets of mouse multipotent hematopoietic stem cells. Proc Natl Acad Sci USA. 1990;87(19):7433–7437. 10.1073/pnas.87.19.7433. [PubMed: 1977160]
37. Chung S, Dzeja PP, Faustino RS, Perez-Terzic C, Behfar A, Terzic A. Mitochondrial oxidative metabolism is required for the cardiac differentiation of stem cells. Nat Clin Pract Cardiovascu Med. 2007;4(S1):S60–S67. 10.1038/ncpcardio0766.
38. Kondoh H, Lleonart ME, Nakashima Y, et al. A high glycolytic flux supports the proliferative potential of murine embryonic stem cells. Antioxid Redox Signal. 2007;9(3):293–299. 10.1089/ars.2006.1467. [PubMed: 17184172]
39. Chen CT, Shih YRV, Kuo TK, Lee OK. Wei YH. Coordinated changes of mitochondrial biogenesis and antioxidant enzymes during osteogenic differentiation of human mesenchymal stem cells. Stem Cells. 2008;26(4):960–968. 10.1634/stemcells.2007-0509. [PubMed: 18218821]
40. Fillmore N, Huqi A, Jaswal JS, et al. Effect of fatty acids on human bone marrow mesenchymal stem cell energy metabolism and survival, PLOS ONE. 2015;10(3):e0120257. 10.1371/journal.pone.0120257. [PubMed: 25768019]
41. Pietilä M, Palomäki S, Lehtonen S, et al. Mitochondrial function and energy metabolism in umbilical cord blood- and bone marrow-derived mesenchymal stem cells. Stem Cells Develop. 2012;21(4):575–588. 10.1089/scd.2011.0023.
42. Flores A, Schell J, Krall AS, et al. Lactate dehydrogenase activity drives hair follicle stem cell activation. Nat Cell Biol. 2017;19(9): 1017–1026. 10.1038/ncb3575. [PubMed: 28812580]
43. Folmes CDL, Dzeja PP, Nelson TJ, Terzic A. Metabolic plasticity in stem cell homeostasis and differentiation. Cell Stem Cell. 2012;11(5):596–606. 10.1016/j.stem.2012.10.002. [PubMed: 23122287]
44. Van Blerkom J Mitochondria in early mammalian development. Semin Cell Develop Biol. 2009;20(3):354–364. 10.1016/j.semcdb.2008.12.005.
45. Johnson MT, Mahmood S, Patel MS. Intermediary metabolism and energetics during murine early embryogenesis. J Biol Chem. 2003;278(34):31457–31460. 10.1074/jbc.r300002200. [PubMed: 12788927]
46. Tsogtbaatar E, Landin C, Minter-Dykhouse K, Folmes CDL. Energy metabolism regulates stem cell pluripotency. Front Cell Develop Biol. 2020;8. 10.3389/fcell.2020.00087.
47. França LR, Silva VA, Chiarini-Garcia H, Garcia SK, Debeljuk L. Cell Proliferation and hormonal changes during postnatal development of the testis in the pig. Biol Reprod. 2000;63(6):1629–1636. 10.1095/biolreprod63.6.1629. [PubMed: 11090429]
48. Foster DL, Hileman SM. Puberty in the sheep. In: Knobil and Neill's Physiology of Reproduction. Vol 2, 4th ed. Cambridge, MA, USA: Academic Press; 2015. 10.1016/B978-0-12-397175-3.00031-4.
49. Kollin C, Stukenborg J- B, Nurmio M, et al. Boys with undescended testes: endocrine, volumetric and morphometric studies on testicular function before and after orchidopexy at nine months or three years of age. J Clin Endocrinol Metabol. 2012;97(12):4588–4595. 10.1210/jc.2012-2325.
50. Al-Ani A, Toms D, Kondro D, Thundathil J, Yu Y, Ungrin M. Oxygenation in cell culture: critical parameters for reproducibility are routinely not reported. PLoS ONE. 2018;13(10):e0204269. 10.1371/journal.pone.0204269. [PubMed: 30325922]
51. Sakib S, Yu Y, Voigt A, Ungrin M, Dobrinski I. Generation of porcine testicular organoids with testis specific architecture using microwell culture. J Visualized Experiments. 2019;152:e60387. 10.3791/60387.
52. Tang L, Bondareva A, Gonzalez R, et al. TALEN-mediated gene targeting in porcine spermatogonia. Mol Reprod Develop. 2018;85(3):250–261. 10.1002/mrd.22961.
53. Melamud E, Vastag L, Rabinowitz JD. Metabolomic analysis and visualization engine for LC-MS data. Anal Chem. 2010;82(23):9818–9826. 10.1021/ac1021166. [PubMed: 21049934]

54. Clasquin MF, Melamud E, Rabinowitz JD. LC-MS data processing with MAVEN: a metabolomic analysis and visualization engine. Curr Protocols Bioinform. 2012;37(1):14.11.1–14.11.23. 10.1002/0471250953.bi1411s37.
55. Huang H, Gao Q, Peng X, et al. piRNA-associated germline nuage formation and spermatogenesis require MitoPLD pro-fusogenic mitochondrial-surface lipid signaling. Develop Cell. 2011;20(3):376–387. 10.1016/j.devcel.2011.01.004.
56. Wang X, Lv C, Guo Y, Yuan S. Mitochondria associated germinal structures in spermatogenesis: piRNA pathway regulation and beyond. Cells. 2020;9(2):399. 10.3390/cells9020399.
57. Picut CA, Ziejewski MK, Stanislaus D. Comparative aspects of pre- and postnatal development of the male reproductive system. Birth Defects Res. 2018;110(3):190–227. 10.1002/bdr2.1133. [PubMed: 29063715]
58. Vodicka P, Smetana K, Dvoránková B, et al. The miniature pig as an animal model in biomedical research. Ann N Y Acad Sci. 2005; 1049(1):161–171. 10.1196/annals.1334.015. [PubMed: 15965115]
59. Plant TM, Terasawa E, Witchel SF. Puberty in non-human primates and man. In: Knobil and Neill's Physiology of Reproduction. Vol 2, 4th ed. Cambridge, MA: Academic Press; 2015: 1487–1536. 10.1016/B978-0-12-397175-3.00032-6.
60. Kosco MS, Loseth KJ, Crabo BG. Development of the seminiferous tubules after neonatal hemicastration in the boar. Reproduction. 1989;87(1):1–11. 10.1530/jrf.0.0870001.
61. Tran D, Meusy-Dessolle N, Josso N. Waning of anti-Müllerian activity: an early sign of Sertoli cell maturation in the developing pig. Biol Reprod. 1981;24(4):923–931. 10.1095/biolreprod24.4.923. [PubMed: 6894705]
62. Oliveira PF, Martins AD, Moreira AC, Cheng CY, Alves MG. The warburg effect revisited-lesson from the Sertoli cell. Med Res Rev. 2015;35(1):126–151. 10.1002/med.21325. [PubMed: 25043918]
63. Divakaruni AS, Paradyse A, Ferrick DA, Murphy AN, Jastroch M. Methods in enzymology. In: Analysis and Interpretation of Microplate-Based Oxygen Consumption and PH Data. Vol. 547. Cambridge, MA, USA: Academic Press; 2014: 309–354. 10.1016/B978-0-12-801415-8.00016-3.
64. Wagner BA, Venkataraman S, Buettner GR. The rate of oxygen utilization by cells. Free Rad Biol Med. 2011;51(3):700–712. 10.1016/j.freeradbiomed.2011.05.024. [PubMed: 21664270]
65. Oliveira PF, Alves MG. Testicular metabolic cooperation. In: Sertoli Cell Metabolism and Spermatogenesis. Cham: Springer; 2015:41–56. 10.1007/978-3-319-19791-3.
66. Jutte NHPM, Jansen R, Grootegoed JA, Rommerts FFG, van der Molen HJ. FSH stimulation of the production of pyruvate and lactate by rat Sertoli cells may be involved in hormonal regulation of spermatogenesis. Reproduction. 1983;68(1):219–226. 10.1530/jrf.0.0680219.
67. Rato L, Alves MG, Socorro S, Duarte AI, Cavaco JE, Oliveira PF. Metabolic regulation is important for spermatogenesis. Nat Rev Urol. 2012;9(6):330–338. 10.1038/nrurol.2012.77. [PubMed: 22549313]
68. Boussouar F, Benahmed M. Lactate and energy metabolism in male germ cells. Trends Endocrinol Metabol. 2004;15(7):345–350. 10.1016/j.tem.2004.07.003.
69. Gac FL, Attramadal H, Borrebaek B, et al. Effects of FSH, isoproterenol, and cyclic AMP on the production of lactate and pyruvate by cultured Sertoli cells. Arch Androl. 1983;10(2):149–154. 10.3109/01485018308987556. [PubMed: 6305294]
70. Goldberg E, Eddy EM, Duan C, Odet F. LDHC: the ultimate testis-specific gene. J Androl. 2010;31(1):86–94. 10.2164/jandrol.109.008367. [PubMed: 19875487]
71. Morimoto H, Kanastu-Shinohara M, Ogonuki N, et al. ROS amplification drives mouse spermatogonial stem cell self-renewal. Life Sci Alliance. 2019;2(2):e201900374. 10.26508/lsa.201900374. [PubMed: 30940732]
72. Moussaieff A, Rouleau M, Kitsberg D, et al. Glycolysis-mediated changes in acetyl-CoA and histone acetylation control the early differentiation of embryonic stem cells. Cell Metabol. 2015;21(3):392–402. 10.1016/j.cmet.2015.02.002.
73. Plant TM, Barker-Gibb ML. Neurobiological mechanisms of puberty in higher primates. Hum Reprod Update. 2004;10(1):67–77. 10.1093/humupd/dmh001. [PubMed: 15005465]

74. Grumbach MM. The neuroendocrinology of human puberty revisited. Hormone Res Paediatr. 2002;57(2):2–14. 10.1159/000058094.
75. Eddy EM. Male germ cell gene expression. Recent Prog Hormone Rese. 2002;57(1):103–128. 10.1210/rp.57.E103.
76. Lord T, Nixon B. Metabolic changes accompanying spermatogonial stem cell differentiation. Develop Cell. 2020;52(4):399–411. 10.1016/j.devcel.2020.01.014.
77. Hayashi Y, Otsuka K, Ebina M, et al. Distinct requirements for energy metabolism in mouse primordial germ cells and their reprogramming to embryonic germ cells. Proc Natl Acad Sci USA. 2017;114(31):8289–8294. 10.1073/pnas.1620915114. [PubMed: 28716939]
78. Lu V, Teitell MA. Alpha-ketoglutarate: a “magic” metabolite in early germ cell development. EMBO J. 2019;38(1):e100615. 10.15252/embj.2018100615. [PubMed: 30275267]
79. Tischler J, Gruhn WH, Reid J, et al. Metabolic regulation of pluripotency and germ cell fate through α-ketoglutarate. EMBO J. 2019;38(1):e99518. 10.15252/embj.201899518. [PubMed: 30257965]
80. Clermont Y, Perey B. Quantitative study of the cell population of the seminiferous tubules in immature rats. Am J Anat. 1957;100(2):241–267. 10.1002/aja.1001000205. [PubMed: 13435229]
81. Ito K, Ito K. Hematopoietic stem cell fate through metabolic control. Exp Hematol. 2018;64:1–11. 10.1016/j.exphem.2018.05.005. [PubMed: 29807063]
82. Shyh-Chang N, Daley GQ, Cantley LC. Stem cell metabolism in tissue development and aging. Development. 2013;140(12):2535–2547. 10.1242/dev.091777. [PubMed: 23715547]
83. Galetzka D, Weis E, Tralau T, Seidmann L, Haaf T. Sex-specific windows for high mRNA expression of DNA methyltransferases 1 and 3A and methyl-CpG-binding domain proteins 2 and 4 in human fetal gonads. Mol Reprod Develop. 2007;74(2):233–241. 10.1002/mrd.20615.
84. Miki K, Qu W, Goulding EH, et al. Glyceraldehyde 3-phosphate dehydrogenase-S, a sperm-specific glycolytic enzyme, is required for sperm motility and male fertility. Proc Natl Acad Sci USA. 2004;101 (47): 16501–16506. 10.1073/pnas.0407708101. [PubMed: 15546993]
85. Bunch DO. Glyceraldehyde 3-phosphate dehydrogenase-S protein distribution during mouse spermatogenesis. Biol Reprod. 1998;58(3):834–841. 10.1095/biolreprod58.3.834. [PubMed: 9510974]
86. Nakamura M, Fujiwara A, Yasumasu I, Okinaga S, Arai K. Regulation of glucose metabolism by adenine nucleotides in round spermatids from rat testes. J Biol Chem. 1982;257(23): 13945–13950. [PubMed: 7142187]
87. Nakamura M, Okinaga S, Arai K. Metabolism of round sperma tids: evidence that lactate is preferred substrate. Am J Physiol-Endocrinol Metabol 1984;247(2):E234–E242. 10.1152/ajpendo.1984.247.2.e234.
88. Ježek P, Holendová B, Garlid KD, Jabůrek M. Mitochondrial uncoupling proteins: subtle regulators of cellular redox signaling. Antioxid Redox Signal. 2018;29(7):667–714. 10.1089/ars.2017.7225. [PubMed: 29351723]
89. Zhang J, Khvorostov I, Hong JS, et al. UCP2 regulates energy metabolism and differentiation potential of human pluripotent stem cells. EMBO J. 2011;30(24):4860–4873. 10.1038/emboj.2011.401. [PubMed: 22085932]
90. Butcher L, Coates A, Martin KL, Rutherford AJ, Leese HJ. Metabolism of pyruvate by the early human embryo. Biol Reprod. 1998;58(4):1054–1056. 10.1095/biolreprod58A1054. [PubMed: 9546739]
91. Morimoto H, Iwata K, Ogonuki N, et al. ROS are required for mouse spermatogonial stem cell self-renewal. Cell Stem Cell. 2013;12(6):774–786. 10.1016/j.stem.2013.04.001. [PubMed: 23746981]
92. Holmström KM, Finkel T. Cellular mechanisms and physiological consequences of redox-dependent signalling. Nat Rev Mol Cell Biol. 2014;15(6):411–421. 10.1038/nrm3801. [PubMed: 24854789]
93. Murphy MP. How mitochondria produce reactive oxygen species. Biochem J. 2009;417(1):1–13. 10.1042/bj20081386. [PubMed: 19061483]

94. Birben E, Sahiner UM, Sackesen C, Erzurum S, Kalayci O. Oxidative stress and antioxidant defense. World Allergy Organ J. 2012;5(1):9–19. 10.1097/wox.0b013e3182439613. [PubMed: 23268465]

95. Korshunov SS, Skulachev VP, Starkov AA. High protonic potential actuates a mechanism of production of reactive oxygen species in mitochondria. FEBS Lett. 1997;416(1):15–18. 10.1016/s0014-5793(97)01159-9. [PubMed: 9369223]

96. Cho YM, Kwon S, Pak YK, et al. Dynamic changes in mitochondrial biogenesis and antioxidant enzymes during the spontaneous differentiation of human embryonic stem cells, Biochem Biophys Res Commun. 2006;348(4):1472–1478. 10.1016/j.bbrc.2006.08.020. [PubMed: 16920071]

97. Pui HP, Saga Y. Saga Y Gonocytes-to-spermatogonia transition initiates prior to birth in murine testes and it requires FGF signaling. Mech Dev. 2017;144:125–139. 10.1016/j.mod.2017.03.002. [PubMed: 28341395]

98. Costoya JA. Functional analysis of the role of POK transcriptional repressors. Brief Funct Genomics Proteomics. 2007;6(1):8–18. 10.1093/bfgp/elm002.

99. Costoya JA, Hobbs RM, Barna M, et al. Essential role of Plzf in maintenance of spermatogonial stem cells, Nat Genet. 2004;36(6):653–659. 10.1038/ng1367. [PubMed: 15156143]

100. Buaas FW, Kirsh AL, Sharma M, et al. Plzf is required in adult male germ cells for stem cell self-renewal, Nat Genet. 2004;36(6):647–652. 10.1038/ng1366. [PubMed: 15156142]

101. Oatley JM, Avarbock MR, Brinster RL. Glial cell line-derived neurotrophic factor regulation of genes essential for self-renewal of mouse spermatogonial stem cells is dependent on Src family kinase signaling, J Biol Chem. 2007;282(35):25842–25851. 10.1074/jbc.m703474200. [PubMed: 17597063]

102. Lee J, Kanatsu-Shinohara M, et al. Akt mediates self-renewal division of mouse spermatogonial stem cells. Development. 2007; 134(10): 1853–1859. 10.1242/dev.003004. [PubMed: 17428826]

103. Honaramooz A, Megee SO, Dobrinski I. Germ cell transplantation in pigs. Biol Reprod. 2002;66(1):21–28. 10.1095/biolreprod66.1.21. [PubMed: 11751259]

104. Barton LJ, LeBlanc MG, Lehmann R. Finding their way: themes in germ cell migration. Curr Opin Cell Biol. 2016;42:128–137. 10.1016/j.ceb.2016.07.007. [PubMed: 27484857]

105. Mauduit C, Hamamah S, Benhamed M. Stem cell factor/c-kit system in spermatogenesis. Hum Reprod Update. 1999; 5(5):535–545. 10.1093/humupd/5.5.535. [PubMed: 10582791]

106. Snyder EM, Small C, Griswold MD. retinoic acid availability drives the asynchronous initiation of spermatogonial differentiation in the mouse. Biol Reprod. 2010;83(5):783–790. 10.1095/biolreprod.110.085811. [PubMed: 20650878]

107. Zhou Q, Li Y, Nie R, et al. Expression of stimulated by ret inoic acid Gene 8 (Stra8) and maturation of murine gonocytes and spermatogonia induced by retinoic acid in vitro. Biol Reprod. 2008;78(3):537–545. 10.1095/biolreprod.107.064337. [PubMed: 18032419]

108. Pellegrini M, Filipponi D, Gori M, et al. ATRA and KL promote differentiation toward the meiotic program of male germ cells, Cell Cycle. 2008;7(24):3878–3888. 10.4161/cc.7.24.7262. [PubMed: 19098446]

109. Puszyk W, Down T, Grimwade D, et al. The epigenetic regulator PLZF represses L1 retrotransposition in germ and progenitor cells. EMBO J. 2013;32(13):1941–1952. 10.1038/emboj.2013.118. [PubMed: 23727884]

110. Hobbs RM, Seandel M, Falciatori I, Rafii S, Pandolfi PP. Plzf regulates germline progenitor self-renewal by opposing mTORC1. Cell. 2010;142(3):468–479. 10.1016/j.cell.2010.06.041. [PubMed: 20691905]

111. de la Cruz López KG, Toledo Guzmán ME, Sánchez EO, García CA. mTORC1 as a regulator of mitochondrial functions and a therapeutic target in cancer, Front Oncol. 2019;9:1373. 10.3389/fonc.2019.01373. [PubMed: 31921637]

112. Ho TT, Warr MR, Adelman ER, et al. Autophagy maintains the metabolism and function of young and old stem cells, Nature. 2017;543(7644):205–210. 10.1038/nature21388. [PubMed: 28241143]

113. Motta PM, Nottola SA, Makabe S, Heyn R. Mitochondrial morphology in human fetal and adult female germ cells. Hum Reprod. 2000;15(suppl. 2):129–147. 10.1093/humrep/15.suppl_2.129.

114. Novi AM, Saba P. An electron microscopic study of the development of rat testis in the first 10 postnatal days. Zeitschrift für Zellforschung und Mikroskopische Anatomie. 1968;86(3):313–326. 10.1007/bf00332472. [PubMed: 5707283]
115. Paniagua R, Nistal M, Amat P, Rodriguez MC. Presence of ribonucleoproteins and basic proteins in the nuage and intermitochondrial bars of human spermatogonia. J Anat. 1985;143:201–206. [PubMed: 3870728]
116. Wang X, Wen Y, Dong J, Cao C, Yuan S. Systematic in-depth proteomic analysis of mitochondria-associated endoplasmic reticulum membranes in mouse and human testes. Proteomics. 2018;18(14):e1700478. 10.1002/pmic.201700478. [PubMed: 29785746]
117. Zagore LL, Sweet TJ, Hannigan MM, et al. DAZL regulates germ cell survival through a network of PolyA-proximal mRNA interactions. Cell Reports. 2018;25(5):1225–1240.e6. 10.1016/j.celrep.2018.10.012. [PubMed: 30380414]
118. Mikedis MM, Fan Y, Nicholls PK, et al. DAZL mediates a broad translational program regulating expansion and differentiation of spermatogonial progenitors. eLife. 2020;9:e56523. 10.7554/elife.56523. [PubMed: 32686646]
119. Li X, Han G, Li X, et al. Mitochondrial pyruvate carrier function determines cell stemness and metabolic reprogramming in cancer cells. Oncotarget. 2017;8(28):46363–46380. 10.18632/oncotarget.18199. [PubMed: 28624784]
120. Ryall JG, Cliff T, Dalton S, Sartorelli V. Metabolic reprogramming of stem cell epigenetics. Cell Stem Cell. 2015;17(6):651–662. 10.1016/j.stem.2015.11.012. [PubMed: 26637942]
121. Harvey A, Caretti G, Moresi V, Renzini A, Adamo S. Interplay between metabolites and the epigenome in regulating embryonic and adult stem cell potency and maintenance. Stem Cell Rep. 2019;13(4):573–589. 10.1016/j.stemcr.2019.09.003.
122. Sun YC, Wang YY, Ge W, Cheng SF, Dyce PW, Shen W. Epigenetic regulation during the differentiation of stem cells to germ cells. Oncotarget. 2017;8(34):57836–57844. 10.18632/oncotarget.18444. [PubMed: 28915715]
123. Eguizabal C, Herrera L, De Onate L, Montserrat N, Hajkova P, Izpisua Belmonte JC. Characterization of the epigenetic changes during human gonadal primordial germ cells reprogramming. Stem Cells. 2016;34(9):2418–2428. 10.1002/stem.2422. [PubMed: 27300161]
124. Zeng Y, Chen T. DNA methylation reprogramming during mammalian development. Genes. 2019;10(4):257. 10.3390/genes10040257.
125. Boussouar F, Goudarzi A, Buchou T, et al. A specific CBP/p300-dependent gene expression programme drives the metabolic remodelling in late stages of spermatogenesis. Andrology. 2014;2(3):351–359. 10.1111/j.2047-2927.2014.00184.x. [PubMed: 24522976]
126. Sasaki H, Matsui Y. Epigenetic events in mammalian germ-cell development: reprogramming and beyond. Nat Rev Genet. 2008;9(2):129–140. 10.1038/nrg2295. [PubMed: 18197165]
127. Trisciuoglio D, Di Martile M, Del Bufalo D. Emerging role of histone acetyltransferase in stem cells and cancer. Stem Cells Int. 2018;2018:8908751. 10.1155/2018/8908751. [PubMed: 30651738]
128. Godmann M, May E, Kimmins S. Epigenetic mechanisms regulate stem cell expressed genes Pou5f1 and Gfra1 in a male germ cell line. PLoS ONE. 2010;5(9):e12727. 10.1371/journal.pone.0012727. [PubMed: 20856864]

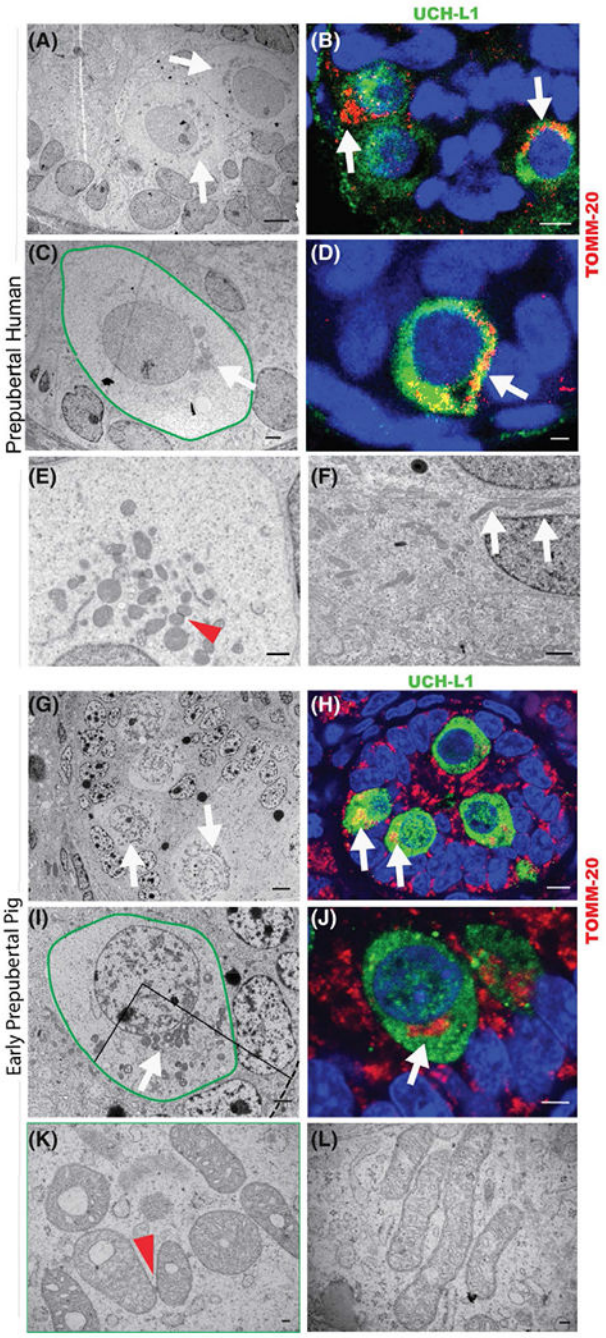

FIGURE 1.

Early prepubertal human and pig spermatogonia have a similar, distinct mitochondrial ultrastructure. A-F, Infant human testis. A, Seminiferous chord in 9-month-old human testis (TEM, white arrows indicate spermatogonia with unilaterally accumulated mitochondria; scale bar 5 μm). B, Seminiferous chord in 6-month-old human testis (IHC for TOMM-20 (red), UCH-L1 (green), white arrows indicate spermatogonia with unilaterally accumulated mitochondria, scale bar 5 μm). C, Early prepubertal (9-month-old human) spermatogonium (green outline) with unilaterally accumulated mitochondria (white arrow), TEM, scale bar 2

μm. D, Early prepubertal spermatogonium (6-month-old human) (IHC for TOMM-20 (red), UCH-L1 (green), white arrow indicates accumulated mitochondria, scale bar 2 μm). E, Mitochondria in early prepubertal spermatogonium (TEM; 9-month-old human, red arrowhead indicates intermitochondrial cement, scale bar 1 μm). F, Mitochondria in early prepubertal Sertoli cell (9-month-old human, white arrows indicate elongated mitochondria, scale bar 1 μm). G-I, Prepubertal pig testis. G, Seminiferous chord in 1-week-old pig testis (TEM; white arrows indicate early prepubertal spermatogonia, scale bar 3 μm). H, Seminiferous chord in 1-week-old pig testis (IHC for TOMM-20 [red], UCH-L1 [green], white arrows indicate spermatogonia with unilaterally accumulated mitochondria, scale bar 5 μm). I, Early prepubertal (1-week-old pig) spermatogonium (green outline) with unilaterally accumulated mitochondria (white arrow), TEM, scale bar 2 μm. Interrupted line indicates the basement membrane, mitochondria mostly accumulated under a 90° angle towards the basement membrane. J, Early prepubertal spermatogonium (1-week-old pig) (IHC for TOMM-20 [red], UCH-L1 [green], white arrow indicates accumulated mitochondria, scale bar 3 μm). K, Mitochondria in early prepubertal (1-week-old pig) spermatogonium (TEM, red arrowhead indicates intermitochondrial cement, scale bar 100 nm). L, Mitochondria in early prepubertal (1-week-old pig) Sertoli cell (TEM; scale bar 100 nm)

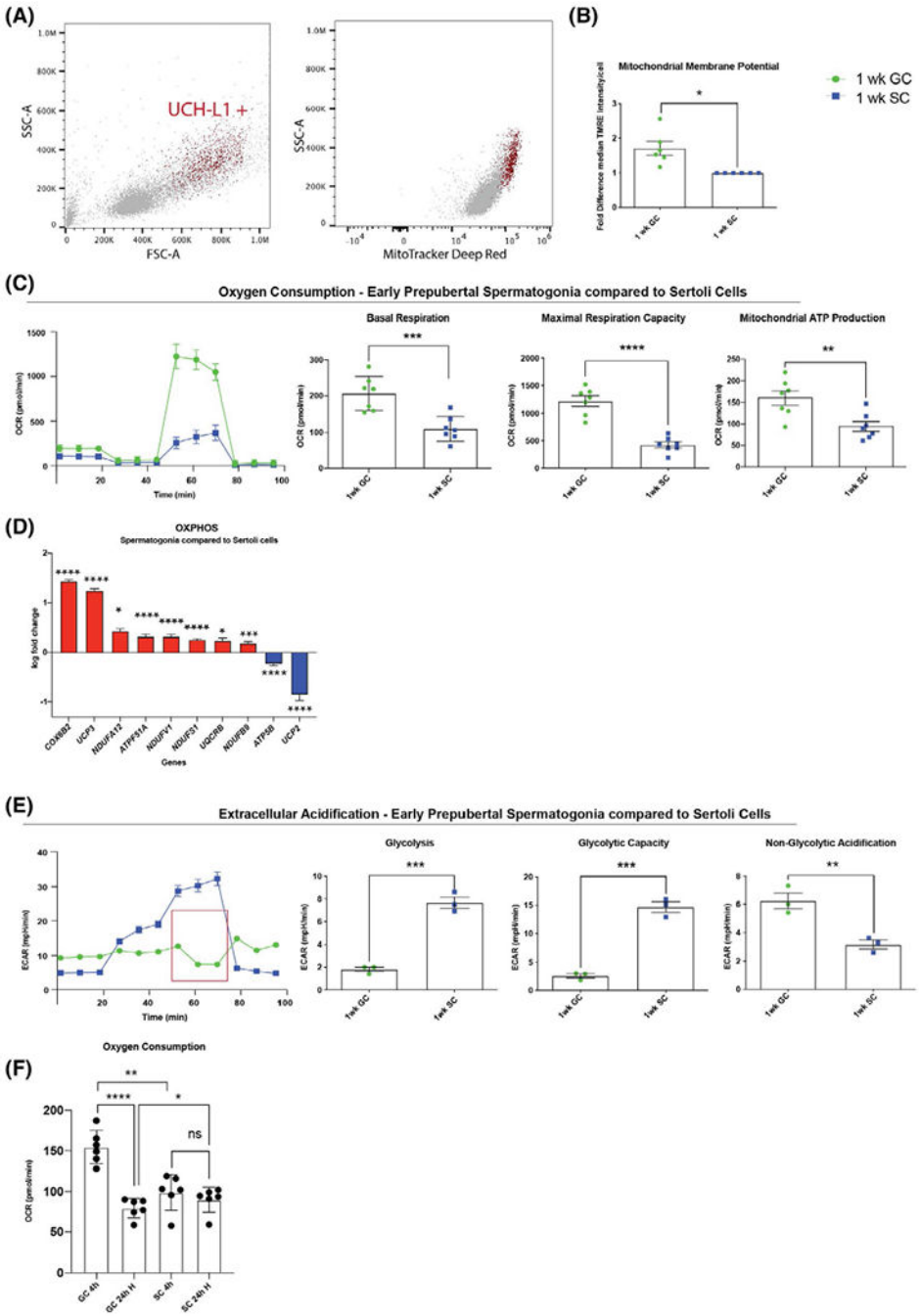

FIGURE 2.

Early prepubertal pig spermatogonia have high mitochondrial activity and low glycolytic capacity. A, Undifferentiated spermatogonia (UCH-L1^{+} red) can be identified in a cell population isolated from seminiferous tubules (grey) by light scatter properties, UCH-L1^{+} cells are MitoTracker Deep Red high and show higher mitochondrial membrane potential than UCH-L1^{-} somatic cells (early prepubertal spermatogonia in red versus testicular somatic cells, majority Sertoli cells, in grey, mean ± SEM of median intensity 126,928 ± 2531 vs 29,553 ± 6070 $P = .0001$, $n = 3$ technical replicates, two-tailed, unpaired Student's t

test). B, Early prepubertal spermatogonia (1-week-old GC) have higher mitochondrial membrane potential than early prepubertal Sertoli cells (1-week-old SC) (mean ± SEM of median intensity of TMRE in flow cytometry $n = 6$; $P = .02$, unpaired Student's t test with Welch's-correction). C, Early prepubertal spermatogonia (green) have higher oxygen consumption rate (OCR) than Sertoli cells (blue) (representative illustration of one biological replicate for OCR assay with the Seahorse Flux Analyzer, mean ± SD, 10 technical replicates); quantification shown as pmol/min/well of 150,000 cells, mean ± SEM; basal respiration ($P = .0008$, $n = 7$); maximum respiration capacity ($P < .0001$, $n = 7$); and mitochondrial ATP production ($P = .006$, $n = 7$) (two-tailed, unpaired Student's t test). D, Early prepubertal spermatogonia show significant upregulation in 8 out of 10 differentially expressed genes compared to Sertoli cells (data shown in log fold change compared to Sertoli cell Δct mean, $n = 4$, $P < .05$). E, Early prepubertal spermatogonia have lower glycolytic activity than Sertoli cells (representative illustration of one biological replicate for extracellular acidification rate [ECAR] assay with the Seahorse Flux Analyzer, mean ± SD of 10 technical replicates); quantification shown as mpH/min/well of 150 000 cells, mean ± SEM, of glycolysis ($P = .0004$, $n = 3$); glycolytic capacity ($P = .0003$, $n = 3$) and nonglycolytic acidification ($P = .0084$, $n = 3$). F, Early prepubertal spermatogonia have significantly higher OCR than Sertoli cells at normoxia (mean ± SEM, $P = .0011$, $n = 6$) but have significantly lower OCR than Sertoli cells after 24 hours of hypoxia (mean ± SEM, $P = .0411$, $n = 6$) and do not recover to the initial OCR after hypoxia (mean ± SEM, $P < .0001$, $n = 6$). Sertoli cells do not show a change in OCR after exposure to hypoxia (mean ± SEM, $P = .14$, $n = 6$; two-tailed, unpaired Student's t test and nonparametric t test

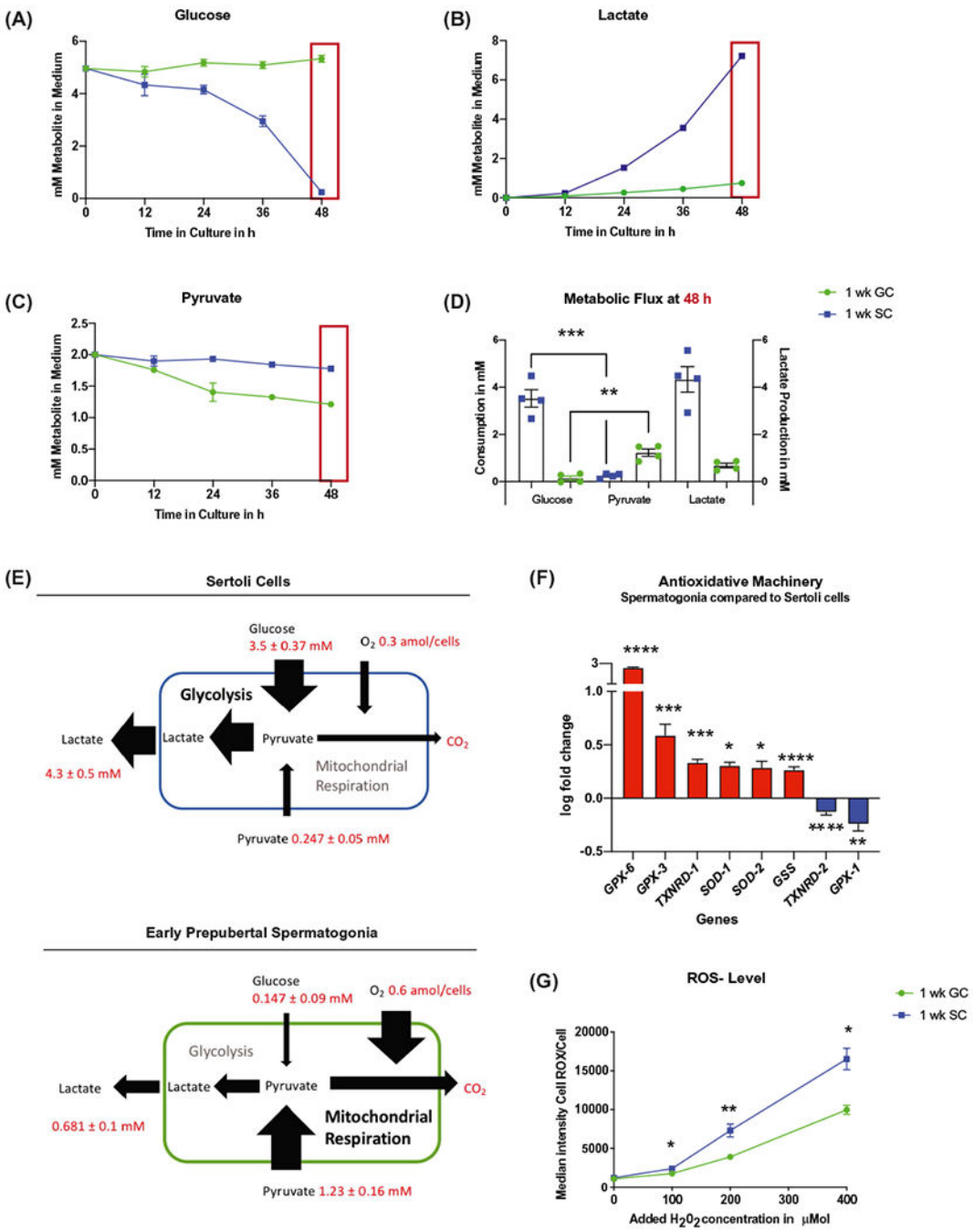

FIGURE 3.

Early prepubertal spermatogonia use pyruvate to fuel OXPHOS and show high antioxidative resistance. A-E, Early prepubertal spermatogonia (GC, green) consume less glucose than Sertoli cells (SC, blue) and higher amounts of pyruvate. A-C, Representative time course of one biological replicate of glucose (A), pyruvate (B), and lactate (C) consumption over 48 hours of culture. D, Consumption of glucose and pyruvate after 48 hours of culture, mean ± SEM; glucose/pyruvate SC ($n = 4$, $P = .0001$); glucose GC/pyruvate GC ($P = .001$, $n = 4$); lactate production after 48 hours of culture (mean ± SEM; two-tailed, unpaired Student's t

test). E, Schematic illustration of metabolic flux in Sertoli cells (blue) and early prepubertal spermatogonia (green) under the experimental conditions tested; values are mean ± SEM after 48 hours of culture for 1 well with 150 000 cells. Oxygen consumption was estimated according to results with the Seahorse Flux analyzer and assumed to be consistent over 48 hours of culture for this illustration. F, Early prepubertal spermatogonia show upregulation of six out of eight differentially expressed antioxidative enzymes ($P < .05$, $n = 4$, Table S1). G, Early prepubertal spermatogonia have higher oxidative resistance than Sertoli cells (mean ± SEM of median intensity of CellROX Green in flow cytometry after increasing concentrations of H_2O_2 from 0 to 400 μMol ($P < .03$, $n = 4$) (two-tailed, unpaired Student's *t* test, with Welch's correction for 200 μMol)

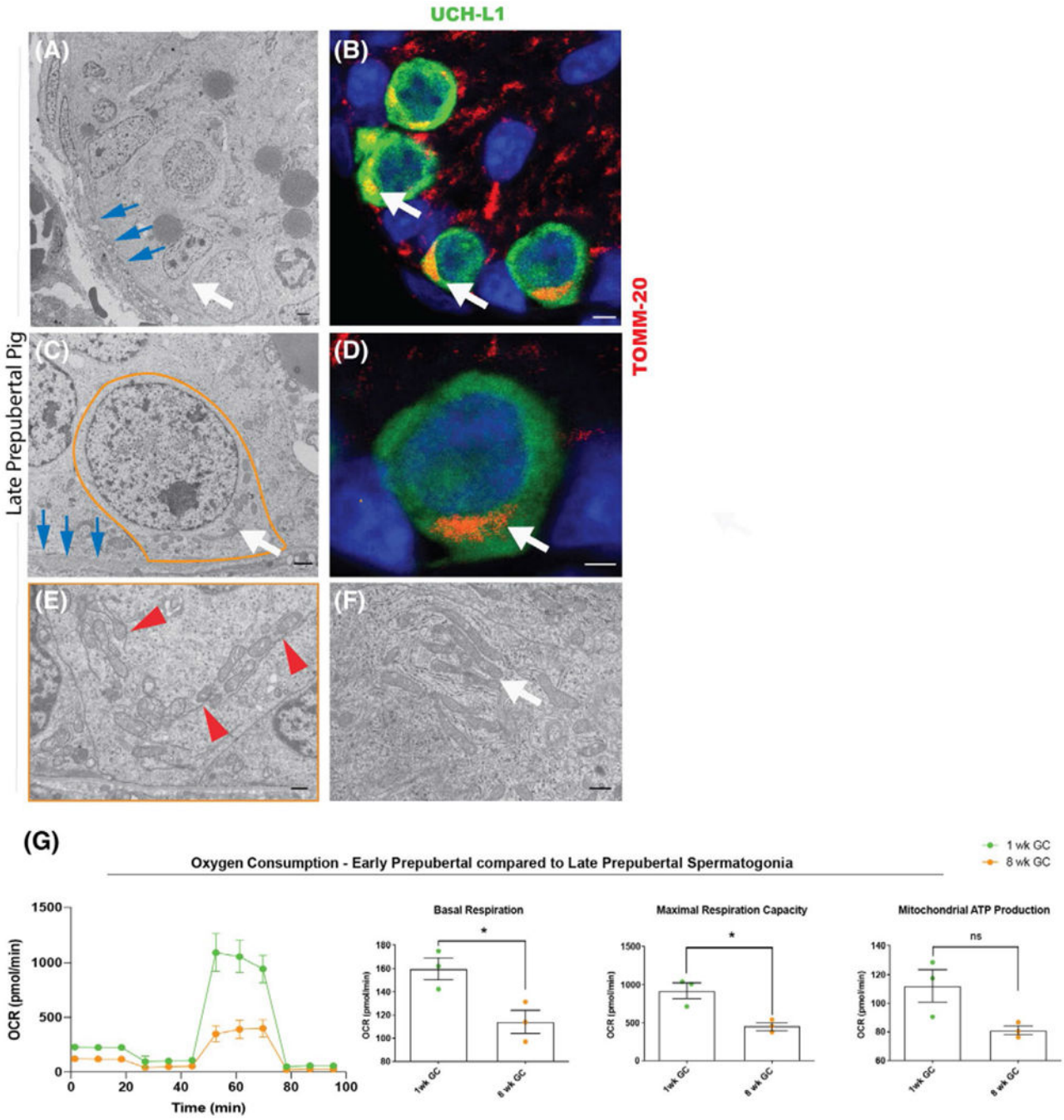

FIGURE 4.

The mitochondrial phenotype changes with spermatogonial maturation. A, Seminiferous chord from 8-week-old pig testis (TEM; white arrow indicates spermatogonia, blue arrow basements indicate membrane, scale bar 2 μm). B, Seminiferous chord from 8-week-old pig testis (IHC for TOMM-20 (red), UCH-L1 (green), white arrows indicate spermatogonia with unilaterally accumulated mitochondria, scale bar 2 μm). C, Late prepubertal (8-week-old pig) spermatogonium (orange outline; TEM; white arrow indicates mitochondria, blue arrow basements indicate membrane, scale bar 2 μm). D, Late prepubertal (8-week-old pig)

spermatogonium IHC for TOMM-20 (red), UCH-L1 (green), white arrow indicates unilaterally accumulated mitochondria, scale bar 2 μm). E, Mitochondria in late prepubertal (8-week-old pig) spermatogonia (TEM, red arrow heads indicate mitochondria associated membranes, scale bar 100 nm). F, Mitochondria in late prepubertal Sertoli cell (white arrow shows elongated mitochondria, scale bar 100 nm). G, Late prepubertal spermatogonia (8 weeks, orange) have lower oxygen consumption rate (OCR) than early prepubertal spermatogonia (1 week, green) (representative illustration of one biological replicate for OCR assay with the Seahorse Flux Analyzer, mean ± SD, $n = 10$ technical replicates); quantification shown as mean ± SEM, basal respiration ($P = .0293$, $n = 3$); maximum respiration capacity ($P = .0155$, $n = 3$); mitochondrial ATP production ($P = .056$, $n = 3$) (two-tailed, unpaired Student's t test)

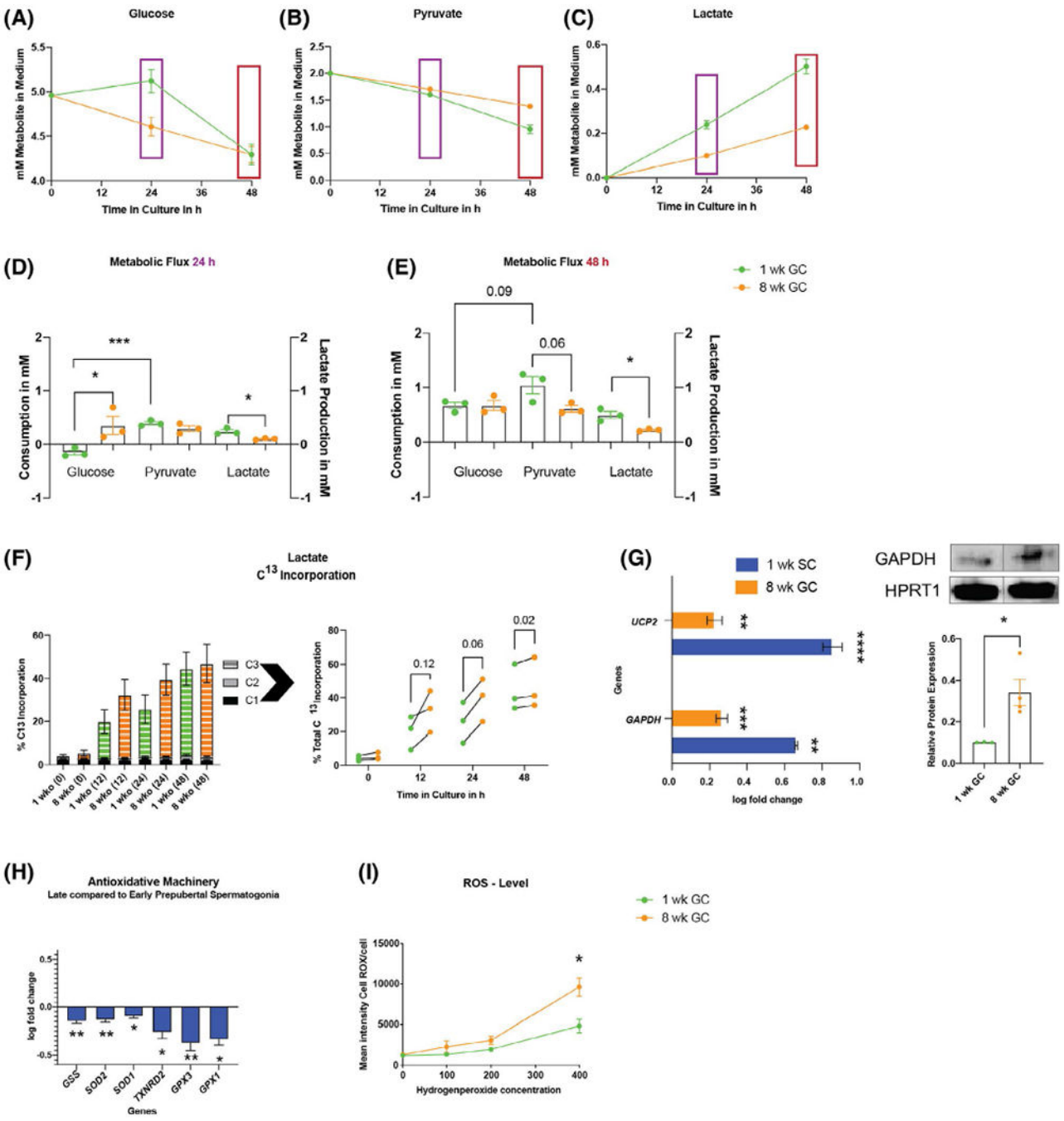

FIGURE 5.

Late prepubertal spermatogonia show a metabolic transition with upregulation of GAPDH and UCP2 and increased sensitivity towards ROS. (A-C) Representative time course of glucose (A), pyruvate (B) consumption, and lactate production (C) in sorted early and late prepubertal spermatogonia in culture. D-E, Mean ± SEM of mM metabolite consumed (left y-axis) (two-tailed, unpaired nested Student's *t* test) and lactate produced (right y-axis) at 24 hours (purple) and 48 hours (red) of culture (two-tailed, unpaired Student's *t* test). F, Percent U-C^{13} incorporation into lactate for early (green) versus late (orange) prepubertal

spermatogonia (stacked values for C1, C2, and C3 incorporation and individual replicates connected with a line for biological replicates of the two ages harvested the same day (values of total incorporation, $n = 3$; P values for fold difference, t_0: 1.32 ± 0.13, $P = .12$; t_{12}: 1.77 ± 0.52, $P = .12$; t_{24}: 1.63 ± 0.17, $P = .06$; t_{48}: 1.052 ± 0.01, $P = .02$). (G) Upregulation of GAPDH and UCP2 in Sertoli cells (1-week SC) and late prepubertal spermatogonia (8-week GC) compared to early prepubertal spermatogonia (mean ± SEM log fold change compared to mean Δct of early prepubertal spermatogonia; statistics performed on raw Δct, $P < .05$, $n = 4$; Table S1); late prepubertal spermatogonia have more GAPDH protein than early prepubertal spermatogonia relative to house keeping protein HPRT1 (outlier identified via ROUT method, mean ± SEM, 0.343 ± 0.065 vs 0.103 ± 0.001 $P = .034$, $n = 3$–4). H, Late prepubertal spermatogonia show significant downregulation of all differentially expressed antioxidative enzymes ($P < .05$, $n = 4$, Table S1). I, Late prepubertal spermatogonia have lower oxidative resistance at high concentrations of hydrogen peroxide (mean ± SEM of median intensity of CellROX Green in flow cytometry after increasing concentrations of H_2O_2 from 0 to 400 μMol; n400 of H_2O_2 ($P = .0268$, $n = 3$) (two-tailed, unpaired Student's t test)

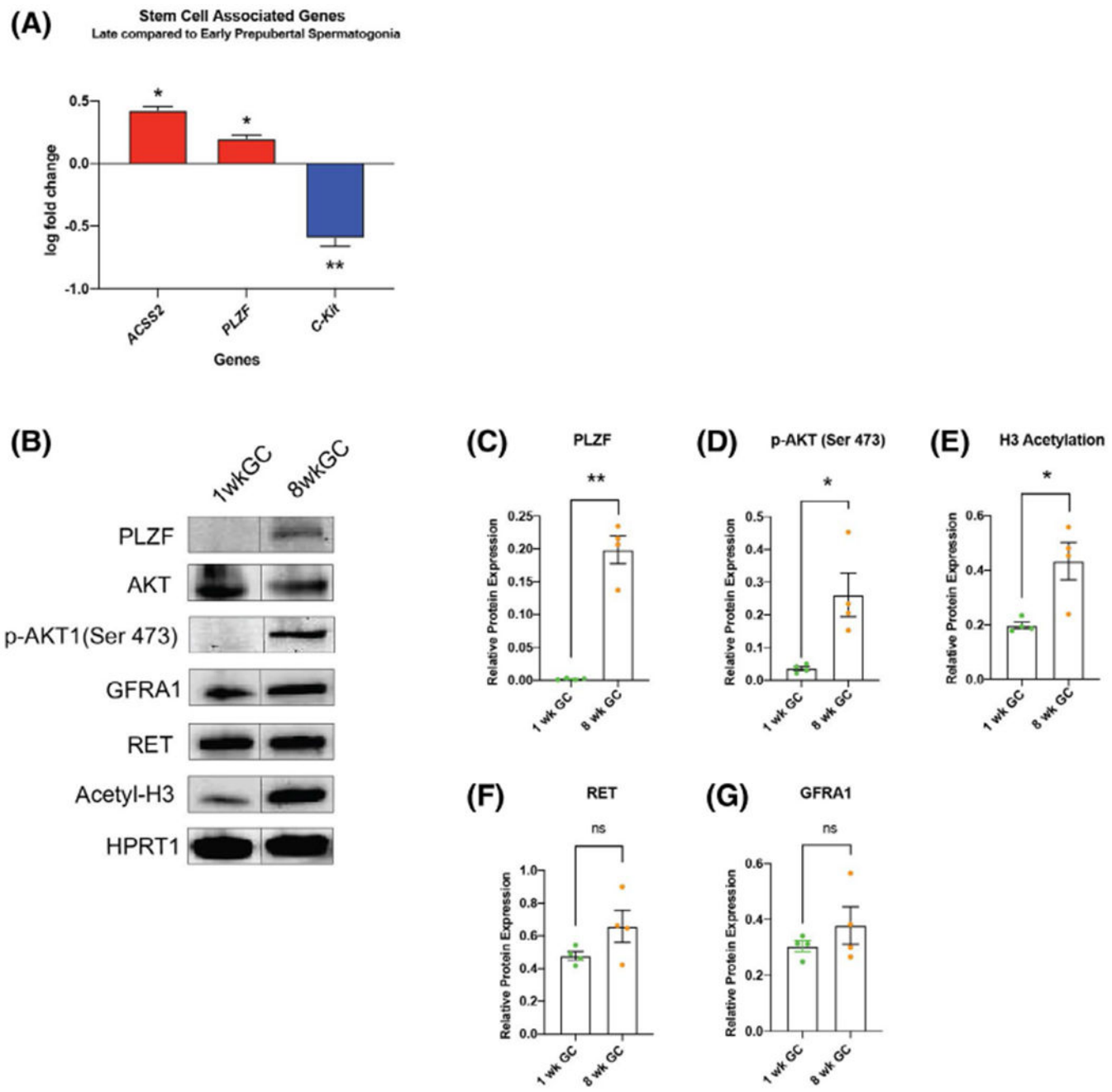

FIGURE 6.

The metabolic shift of late prepubertal spermatogonia is associated with AKT-pathway activation, expression of PLZF and epigenetic changes. A, Late prepubertal spermatogonia show higher expression of ACSS-2 and PLZF, downregulation of C-Kit compared to early prepubertal spermatogonia (mean ± SEM log fold change compared to mean Δct of early prepubertal spermatogonia; statistical analysis performed on raw Δct, $P < .05$, $n = 4$; Table S1). B, Representative image of Western blot analysis of sorted early versus late prepubertal spermatogonia for GAPDH, GFRA1, RET, PLZF, Acetyl-H3 relative to HPRT1. C-G, Quantification early versus late prepubertal spermatogonia; mean ± SEM: (C) PLZF

expression ($P = .0027$, $n = 4$). D, Phosphorylation of AKT (Ser 473) relative to pan AKT ($p = .042$, $n = 4$), E, pan H3 acetyl ($P = .039$, $n = 4$), F, RET ($P = .125$, $n = 4$) and G, GFRA1 ($P = .324$, $n = 4$) (two-tailed, unpaired Student's t test)